ACS APPLIED MATERIALS & INTERFACES

Article

Graphene Oxide-Polycarbonate Track-Etched Nanosieve Platform for Sensitive Detection of Human Immunodeficiency Virus Envelope Glycoprotein

Anuj Nehra, Weizao Chen, Dimiter S. Dimitrov, Anu Puri, and Krishna Pal Singh

ACS Appl. Mater. Interfaces, **Just Accepted Manuscript** • DOI: 10.1021/acsami.7b12103 • Publication Date (Web): 06 Sep 2017

Just Accepted

ACS Publications

ACS Applied Materials & Interfaces is published by the American Chemical Society.
1155 Sixteenth Street N.W., Washington, DC 20036

Graphene Oxide-Polycarbonate Track-Etched Nanosieve Platform for Sensitive Detection of Human Immunodeficiency Virus Envelope Glycoprotein

Anuj Nehra,[‡†] Weizao Chen,[§] Dimiter S. Dimitrov,[§] Anu Puri,[‖] and Krishna Pal Singh,[‡†*]

[‡]Bio-Nanotechnology and Nanobiosensor Research Laboratory, Biophysics Unit, CBSH, G.B. Pant University of Agriculture & Technology, Pantnagar, 263145 U.S. Nagar, Uttarakhand, India, [†]Department of Molecular Biology, Biotechnology and Bioinformatics, Chaudhary Charan Singh Haryana Agriculture University, Hisar, 125004, Haryana, India [§]Cancer and Inflammation Program, Center for Cancer Research, [‖]Gene Regulation and Chromosome Biology Laboratory, NCI, NIH, Frederick, MD, U.S.A 21702-1201.

ABSTRACT:

Solid-state nanopores within graphene-based materials are on the brink of fundamentally changing the sensing of desired bio-analytes through ion trafficking across nanoporous membranes. Here, we report on a two-electrode electrochemical biosensor comprised of a graphene oxide-polycarbonate track-etched nanosieve platform for the rapid and sensitive detection of the Human Immunodeficiency Virus Type 1 (HIV-1) envelope glycoprotein ectodomain ($gp140_{MS}$). We have covalently linked an engineered high-affinity one-domain soluble CD4 fused to a human domain targeting HIV-1 coreceptor binding site and ferrocene (Fc) (2Dm2m) to the nanosieve platform. An exponential decrease in the ionic current resulted from a partial blockade of the nanosieve due to the specific interactions of $gp140_{MS}$ with the 2Dm2m protein, which was immobilized on the nanosieve platform by bio-linkage as a function of applied voltages of 0.1-2.0 volts. There was no change in current when a non-specific antigen bovine serum albumin was tested under identical conditions. This platform had high sensitivity, and when the receptor-binding phenomenon was tested to identify the minimum concentration of target analyte the lowest detection limit was as short as 8.3 fM, and with sensitivity and response times of 0.87 mA-$mM^{-1}cm^{-1}$ and 12 s, respectively. In addition to this remarkable sensitivity, our nano-biorecognition platform has the advantage of superior stability due to the few layered graphene oxide laminates. It also exhibits exceptional biomolecule binding and higher reusability, sustainability and ease of fabrication in a soft mechanism. Real samples of HIV positive and negative patients were successfully tested to confirm the virus by the developed platform. To the best of our knowledge, this is the first time prosperous pervious remembrance surface has been employed in a nano-biosensing application. In light of the recent great trend of using graphene-based nanopore surfaces created by sophisticated ion-beam methods in sensing and sequencing, this hybrid-surface nanolayer fabricated by the simple vacuum filtration of a few layered graphene oxide laminates may serve as a good alternative in terms of ease of fabrication without expensive instrumental prerequisites.

KEYWORDS: nanomaterials, few layered, graphene oxide laminates, nanosieve, HIV protein

INTRODUCTION

Acute advancement in nanotechnology and the importance of nanomaterials[1] have led to an immense curiosity in two-dimensional nanomaterials, such as molybdenum disulfide (MoS_2), graphene,[1,2] noble metals (*e.g.,* Au, Pd and Rh), metal oxides[3] (*e.g.,* TiO_2, WO_3, CeO_2, In_2O_3, SnO_2, Fe_2O_3), and metal chalcogenides (*e.g.,* PbS, CuS, CuSe, SnSe, ZnSe, ZnS, CdSe).[4] One of these graphene is a prominent zero-band-gap layered semiconductor with merits such as high surface area (2630 m^2/g), large intrinsic mobility (200,000 cm^2/vs), good thermal conductivity (~5000 W/mK), optical transmittance (~97.7 %),[5] higher electrical conductivity,[6] environmental sensitivity,[2] and easy preparation. Due to these properties, researchers are using it in many areas, including nanotechnology. Currently, methods such as the modified Hummer's method are available to chemically modify carbon atoms[6,7] in graphene to make newer nanomaterials such as graphene oxide (GO). GO has arisen as a pioneer graphene-based nanomaterials[6] which offers unique advantages like cost effectiveness, functionality,

and various applications. The physical and chemical properties of GO have been used for the growth of well effective membranes having nanochannels or pores for filtration and separation.[8–10]

Recently, graphene and GO have drawn attention for promising applications in sensing[11,12] and separation. However, graphene-based membranes having nanopores generated by an electron beam are very adulterated and need a lot of sophisticated instrumentation, which limits their use. GO membranes congregated using micrometre-structured of GO layers can have conspicuous characteristics such as hydrophilism, excellent mechanical competence, and good flexibility. They are hence optimal candidates for filtration and sieving applications at the nanoscale level.[13–16] Up to now, various methods for GO membranes have been researched.[17–20] For instance, Geim and co-workers demonstrated sub-micrometre free-standing GO membranes as a new-generation nanomaterial platform for high-efficiency separation with gases,[21–24,] water,[8,17,25–28] and ions,[29–32] including He, H_2, N_2, and Ar[8,30] transport channels. These insights properties offer a broad variety of applications for molecular permeation in aquatic conditions or for separating liquid[33] and gas amalgams.[21–24]

Nanoporous graphene[34–37] and GO membranes/films[8,38–40] are currently used for the erection of well-designed optimal biosensing devices such as nano-fluidic electrochemical biosensors (nECBs).[41,42] But the nano-channels present in between the laminates or layers of GO membranes have huge potential for biosensing of biomolecules or proteins. Furthermore, a free-standing GO membrane[43,44] disappears relatively flabbily during the separation process conditions and handling, which can be the greatest extent of thinkable applications. In this manuscript, we fabricated few-layered GO laminates[29,39] immobilized on a PCTE nanoporous membrane as a novel biosensor device.

Currently, the acquired immunedeficiency syndrome (AIDS) epidemic is a world-wide problem, and its severity is further complicated by opportunistic infections, especially in immune-compromised patients. Co-infecting pathogens have been documented to affect AIDS progression and hence contribute to patient morbidity. Recently, Lam et al. demonstrated the capability of microcantilever deflection biosensors to detect the HIV-1 envelope glycoprotein (Env) gp120 *via* monoclonal antibodies (mAbs) A32 or T8 over the exposed surface of microcantilever that is activated by polyethylene glycol chemistry. After incubation with mAbs 17b (mAbs 17b are known to bind an A32-induced epitope on gp120) over the gp120, further increase in the deflection of A32- was observed, but this was not applicable to T8-presenting microcantilever. The researchers used a gp120 concentration of 8 $\mu g.mL^{-1}$ and 0.17 $mg.mL^{-1}$ of 17b. This biosensor showed the minimum detection limit (i.e., less than 400 $ng.mL^{-1}$).[45] Lee et al. reported a novel electrochemical method to detect HIV-1 based on electron transfer signal. In this method, gold nanoparticles were coated on an Indium Tin Oxide glass (ITO) electrode by electrochemical deposition process to enhance the surface area and thereby support enhanced electron-transfer signals as well as higher background of charging current. Afterwards, antibodies corresponding to HIV-1 virus were immobilized over the exposed surface area of the fabricated electrode (ITO) *via* gold-thiol interaction by self-assembly method. This electrode, containing antibody sensors, was then used to direct monitoring of HIV-1 Virus like nanoparticles (VLPs) with different concentrations. This sensor successfully determined HIV-1 VLPs from 600 fg/mL to 375 pg/mL.[46] Furthermore, comparative study depicted in Table 2, reveals several types of modified platforms of electrochemical biosensors analyzed on the basis of detection limit and dynamic range.

We have developed GO-based nanosensors for the detection of purified HIV-1 envelope glycoprotein ($gp140_{MS}$, CLADE A, R5 tropic) as a model system. As a ligand of HIV-1, we have used a bispecific tetravalent human engineered antibody domain (eAd)-sCD4 fusion construct (2Dm2m) that contains an Fc portion for successful conjugation on the GO surface. 2Dm2m targets a highly conserved CD4 binding-induced epitope on HIV-1 and neutralizes various HIV-1 isolates with high affinity,[47–49] as shown in scheme 1. The devices are coated with a high-affinity engineered CD4 domain protein (an HIV-1 envelope glycoprotein gp120-gp41 binding protein (specific)). We have demonstrated that to be an enchantment different class of nanobiosensors to detect HIV-1 $gp140_{MS}$, an antigen for capturing HIV-1. The fundamental theory conceptualized here is very ingenious: when ions move through the GO laminate nanosieve (~pore size 0.45 nm,[29] less than 1 nm[22] and thickness 1 μm[43] to less than 10 μm[31]) by using an external electric field, it procreates some alternate changes in the ionic

current, for scanning one of the ions along its length. Therefore, GO laminates functionalized by 1-ethyl-3-(3-dimethyl aminopropyl) carbodiimide (EDC)-N-hydroxysuccinimide (NHS) working as a nanosieve seem like a good biosensing platform.[29,50] A schematic diagram of the functionalization of GO-PCTE nanoplatform is given in scheme 2.

We present the facile erections of the few-layered GO-PCTE membrane with nanoporous entities between GO layers. We combined this with a 2Dm2m (HIV) receptor fitted between two half cells flings having two Ag/AgCl electrodes. We call this device a nanosieve-assisted electrochemical nanobiosensor and used for detection of purified proteins and real samples.

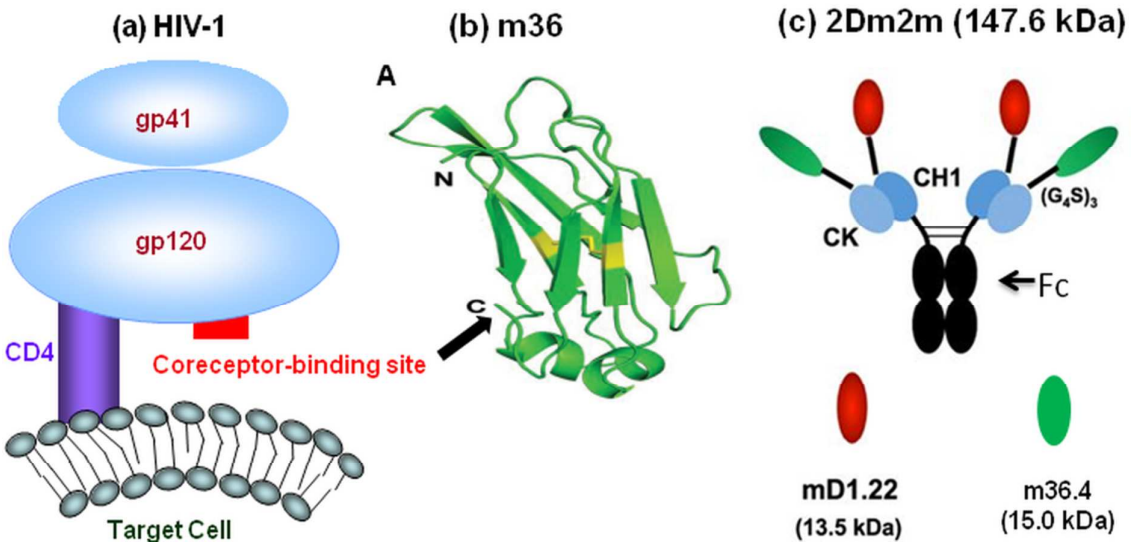

Scheme 1. Show the diagram of **(a)** HIV-1 **(b)** m36 ($gp140_{MS}$), and **(c)** 2Dm2m (CD4).

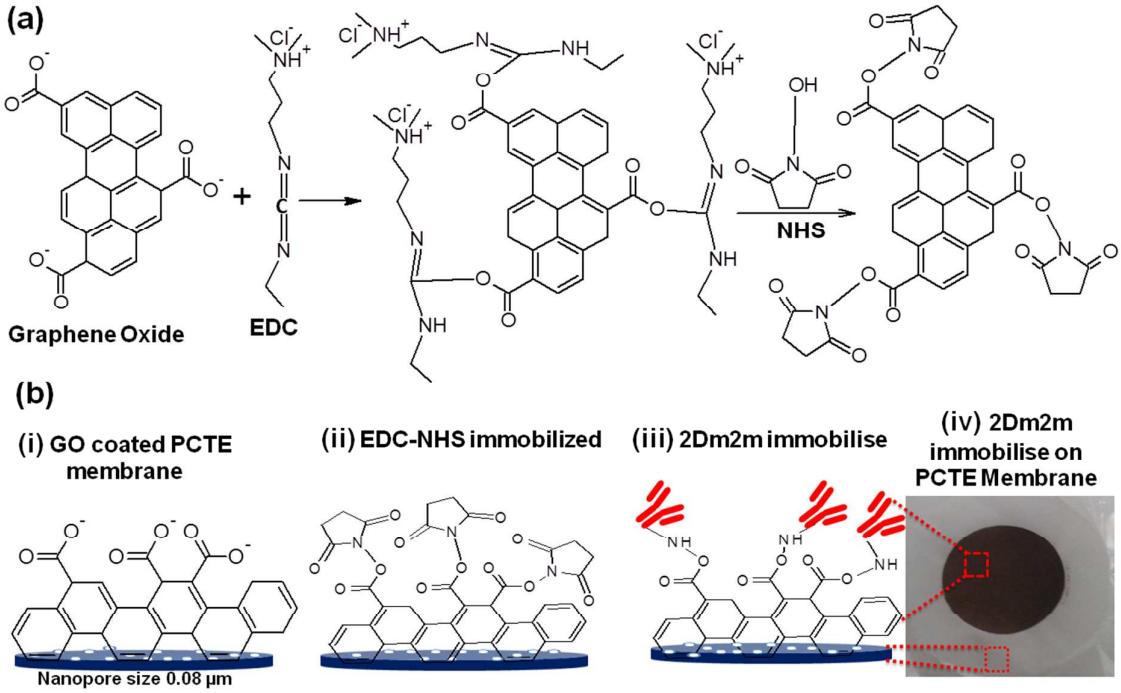

Scheme 2. (a) GO with EDC-NHS linker. **(b)** Immobilized 2Dm2m *via* EDC-NHS on GO coated PCTE membrane.

.

EXPERIMENTAL SECTION

Materials. Sulphuric acid (assay NLT 97.0 %), potassium per sulphate GR (assay 98.0%), phosphorus pentoxide GR (assay 98%), potassium permanganate (assay 99%), hydrogen peroxide (30%) and graphite powder were purchased from Rankem, Molychem, Qualigens, Loba chemie and Aldrich respectively, these chemical was used in GO preparation. In addition, sodium chloride, potassium chloride, sodium hydrogen phosphate, potassium dihydro phosphate, and hydrochloric acid were purchased from Sigma-Aldrich for making the 0.01 M phosphate buffer saline. Nuclepore Track-Etch Membrane (pore size = 0.08 µM, and diameter = 13 mm) was purchased from Whatman. Furthermore, EDC (MW = 191.7 g/mol) and NHS (115.09 g/mol) were purchased from Sigma-Aldrich. 2Dm2m CD4 construct (MW = 147.6 kDa, CC = 4 mg/ml), HIV-1 $gp140_{MS}$ (MW = 140 kDa, CC = 0.3 mg/ml) were prepared, purified and characterized following Chen et al 2014.[48,49] Protein samples were stored in the freezer at – 20 °C before use our research lab. Four HIV positive and two HIV negative human serum samples (see the supporting information Figure S1) were provided by Jindal Institute of Medical Sciences Hospital, Hisar, Haryana, India. The concentration of serum samples were analyzed using Bradford protein assay method by Multiskan GO microplate spectrophotometer (Thermo Scientific) in Biosafety Level-3 (BSL-3) Laboratory facility of National Research Centre on Equines (NRCE), Hisar, Haryana, India. The total protein concentrations in HIV positive human serum samples (P1, P2, P3 and P4) were found to be 46.25 g/L, 46.17 g/L, 75.92 g/L, 60.83 g/L while for HIV negative samples (N1 and N2) it was observed as 74.75 g/L, 77.86 g/L.

Preparation of Ag/AgCl. Here, we have easily prepared Ag/AgCl electrode in our laboratory in different variety shape and size. First, we were cleaned by being swilled with abrasive paper and the swabbed with ethanol (4 mm side of the square and wide 0.3–0.4 mm as per required). Further, two Ag/AgCl wire were mounted in the beaker with a fill of 0.1 M hydrochloric acid, so that these wires were immersed in this solution without touching each other. One wire was connected to the positive terminal and another one to the negative terminal with applied constant voltage 2V with max current 10 mA for 30 min using interactive source meter 2450. According to this phenomenon, current is admitted to flow the chloride ion move to the positive terminal and hydrogen ion to the negative terminal as a bubble of H_2 gas. The chloride coating was uniformed over the surface of the silver wire and got the dark gray-purple color.

Synthesis of Few-Layered GO-Laminates. GO was synthesized by the oxidation of natural graphite powder (GP) according to the modified Hummer's method.[51,52] GP (2.0 g) was accumulated in concentrated sulfuric acid (3.0 mL), potassium persulfate (1.0 g), and phosphorus pentaoxide (1.0 g) at 80℃ for 6 h in a hot air oven. This material was cooled down to room temperature and diluted with 200 ml of distilled water. It was then seeped through filter paper and purified to remove the residual acid until neutral pH. This aqueous solution was subjected to desiccation in a desiccator chamber for three days at room temperature. The desiccated preoxidized graphite powder (PGP) was subjected to oxidation using the standard Hummer's method. Typically, the formation of PGP was accompanied by mixing with concentrated sulfuric acid (23 mL) under constant stirring in an ice bath (~ 8℃).

Under shaking, potassium permanganate (3 g) was added to maintain a constant temperature of the suspension lower than 20℃. The reaction system was subjected to constant stirring while the adding extra distilled water (47 mL) at 35℃ for about 2 h. More distilled water (14 mL) was added after 15 min, and the mixture was stirred for 30 min at 35℃. Then 2.5 mL of hydrogen peroxide (30%) was added to terminate the reaction. The color of the mixture was dark brown to yellow. The mixture was filtered using Whatman filter paper and rinsed out with a 1:10 solution of hydrochloric acid to partially remove the metal ions. The resulting solid was washed and centrifuged at 10,000 rpm for 10 min repeatedly until the pH of the distilled water was adjusted to neutral. The resulting brown GO material was dried at room temperature and then diluted in 100 mL distilled water, stirred for 12 h, and bath sonicated for 8 h for exfoliation. The obtained GO dispersion (1 mg/mL) was again centrifuged at

10,000 rpm for 3 min to separate the unexfoliated GO from the transparent GO dispersion solution (see the supporting information Figure S2).

Fabrication of the nanosieve GO laminates platform with 2Dm2m and gp140$_{MS}$. In the present work, first, the GO was prepared by the modified Hummer's method. As a result the brown pasty materials of GO were formed. The obtained GO (100 mg) was dissolved in 100 mL distilled water and bath sonicated for 8 hours to peel it to GO. Further, this GO dispersion solution was again centrifuged at 10,000 rpm for 3 min to recapture the unexfoliated graphite. The get GO dispersion solution has then changed the concentration 1 to 0.3 mg/ml (see the supporting information Figure S3). The present GO dispersion was coated on PCTE membrane using vacuum filtration unit at variable pressure, which flows rate of the first drop, second, third, fourth, fifth, and so on of the GO dispersion is 92s, 133s, 160s, 210s, 250s, and so on respectively. Thus, GO-laminates PCTE membrane was obtained in our laboratory (see the Supporting Information Figure S4). Moreover, the functionalization method is depicted in scheme 1. The functionalized GO-laminates were activated using 100 µl (100 mM) of EDC-NHS over 2h at room temperature. The unreacted EDC-NHS was eliminated by the rinsing it with deionised water. Subsequently, the 2Dm2m protein (40 µg/ml in PBS) was immobilised on the EDC-NHS GO-laminates surface over 8 h at room temperature. Afterward, this platform was rinsed with the same PBS solution whereby it is made, finally, gets the desired 2Dm2m-immoblised GO-laminates nanosieve platform and was then transferred to the solution chamber. 100 µl of gp140$_{MS}$ protein was pipetted dropped into the nanosieve platform for each concentration and was then easy to detect.

Instrumentation. All electrical measurement was conducted with Keithley 2450 interactive source meter and Ag/AgCl electrode prepared in our laboratory. A liquid chamber (4 mL volume) was manufactured and used for liquid (Phosphate Buffer Saline with pH 7.2) based detection. The alteration current was normalized as $\Delta I/I_o = (I - I_o)/I_o$, where I_o is the initial ionic current and I is the calculated value in real time, respectively. Fourier transform infrared spectroscopy (FTIR) spectra were collected with an attenuated total reflectance (ATR) (Thermo Fisher Nicolet 6700), and UV-visible spectrophotometer (UV-Vis) spectra were collected with single beam spectrophotometer (Thermo Scientific multiscan GO micro plate reader with cuvette). Furthermore, X-ray diffractometer (XRD), Atomic force microscopy (AFM) and Thermogravimetric/differential thermal analyzer (TG/DTA) spectra were collected from Rigaku, Veeco 5 and Perkin Elmer Diamond TG/DTA respectively. Field Emission Scanning Electron Microscope (FESEM) images and Energy-dispersive X-ray (EDX) spectroscopy data were collected from Tescan Mirab3 instrument.

RESULTS AND DISCUSSION

Characterization of Graphite Powder and GO. The identity of the graphite powder and GO was confirmed using FTIR-ATR, a single beam UV-Vis, an XRD, and a TG/DTA. Figure 1 shows the FTIR-ATR and UV-Vis spectra results of GO. The sample scan spectrum from the FTIR-ATR analysis demonstrates the occupancy of functional groups in the graphite powder (black line) and GO (red line), such as O-H (~3369.46 cm^{-1}) and C=C (~1646.37 cm^{-1}) from unoxidized sp^2 CC bonds,[53] as well as C=C (~1541 cm^{-1}), C=O (~1646.99 cm^{-1}), C-O (1230 cm^{-1}), and C-O-C (~1016.46 cm^{-1}) bonds[20] as shown in Figure 1a. The O-H stretching vibrations in the around 3374.91 cm^{-1} [51,54,55] are ascribed to the hydroxyl and carboxyl groups of GO[56,57] and leftover water in GO layers. Hydrophilic functional groups are also present, such as oxygen-containing GO sheets with improved dispersibility in distilled water.

Figure 1b shows the UV-visible spectrum of the aqueous dispersion of GO. This spectrum demonstrates a predominant absorption peak at 230 nm, which represents the π-π* transition of C=C bonds, and one peak at 290-300 nm, which represented the n-π* transition of C=O bonds. The general characteristics of this spectrum are equivalent to that of previous GO synthesized using the modified Hummer's method, and its adsorption peaks are the same as in the previous literature. The concen-

tration of the centrifuged solution of GO was confirmed by the linear spectrum, which is shown in the supporting information in Figure S3.

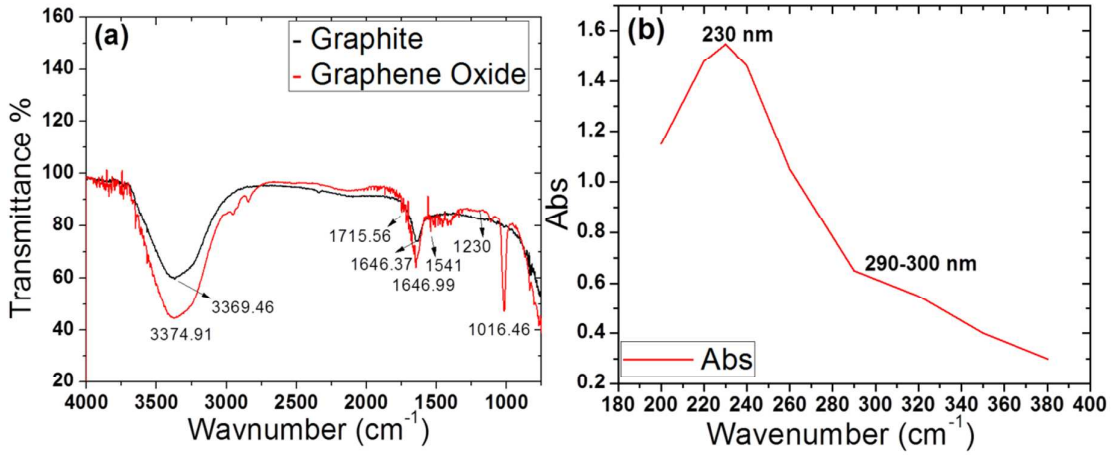

Figure 1. (a) FTIR-ATR spectra of graphite powder (black line) and GO (red line). (b) UV-visible spectrum of an aqueous dispersion of the GO (1 mg/ml).

Next, we analyzed the degree of oxidation and the plane distances between the atoms of graphite powder and GO by powder XRD, as shown in Figure 2a. The XRD pattern was sensitive to the interlaminar microenvironment and the design and oxidation conditions of the layered nanomaterials. The alterations in the spacing between the layers may indicate disruption of functional groups containing bound oxygen in the GO and graphite sheet. The XRD pattern of the normal freeze-dried graphite powder presented peaks at 2θ of 26.4°, 44.4°, and 54.5° corresponding to (002), (101), and (004) planes, respectively (Figure 2a). In the inset Figure 2a, dried GO powder exhibits reflection peaks located at 10.05° and 42.4° corresponding to d-spacing of 0.88 and 0.21 nm, which are the same as previously reported in the literature.[6,51,53,54,58] The large immense spacing between the layers of GO sheets is ascribed to the functional groups of the oxygenated from the oxidation of the graphite powder. The spacing is very helpful for movement of ions through the GO.

The TG/DTA curves of graphite powder and GO are shown in Figure 2b. Herein, both graphs present different characteristics. The first graphite powder weight loss between 500°C and 600°C is ascribed to moisture on the graphite powder layer (Figure 2b). The inset image of Figure 2b shows weight loss before 100°C due to the liberation of captured water molecules between the interlayer sheets of GO.[53,54,59] The weight loss between 150°C and 220°C is ascribed to the breakdown of the fewer stagnant oxygenated functional groups on the GO layers.[54] Debilitated mass losses in the range of 450 to 530°C are ascribed to the elimination of additional stable functional groups. Usually, the TG/DTA curves of the graphite powder sample reflect their far-out contents of oxygenated groups, and the curves of the GO sample reflect their near contents of oxygenated groups.

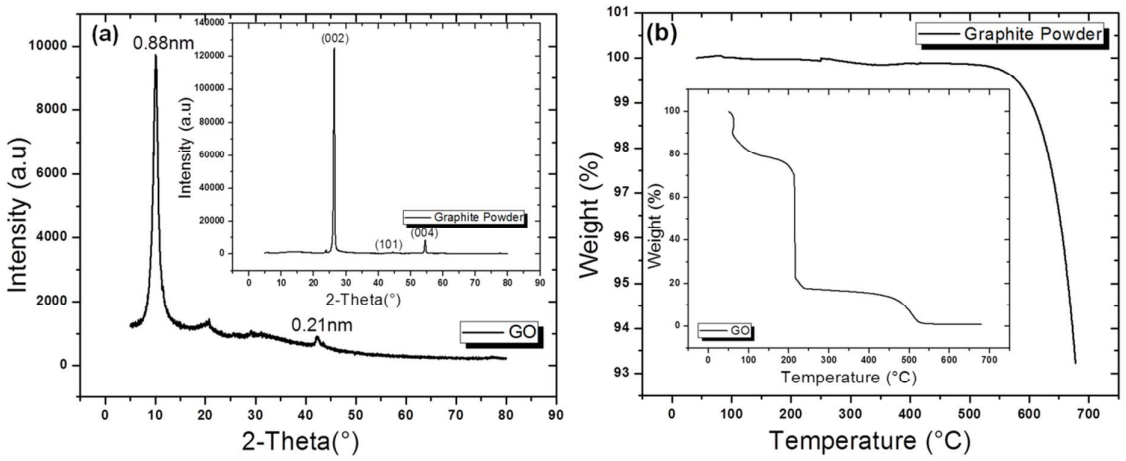

Figure 2. **(a)** XRD pattern of graphite powder showing the (002), (101), and (004) planes. Inset: a corresponding line graph of the GO pattern showing the interlayer d-spacing 0.88 nm and 0.21 nm. **(b)** TG/DTA curves of the dried graphite powder from room temperature to 800°C at a scanning rate of 5°C/min. Inset: TG/DTA curve of the dried GO in the same conditions.

Formation of Nanoporous Few GO-Laminates on PCTE Membrane. The synthesized few-layered GO-laminates were applied to the 6-µm-thick PCTE membrane by a simple vacuum filtration method using Millipore assembly to control the thickness[60] as shown in scheme 3. First, a 0.3 mg/ml GO suspension was sonicated by an ultrasonic bath at 25℃ for 8 hours to convert the remaining pile of GO to single- and few-layers GOs. Then 1 mL of the GO dispersion was placed in a filtration unit and filtered at room temperature with a flux rate of 11.32 L/m^2.h. During the filtration process, the nanoporous GO-PCTE nano membrane dispersion was added drop wise lightly atop the PCTE membrane to confirm an orderly distribution everywhere on the surface.

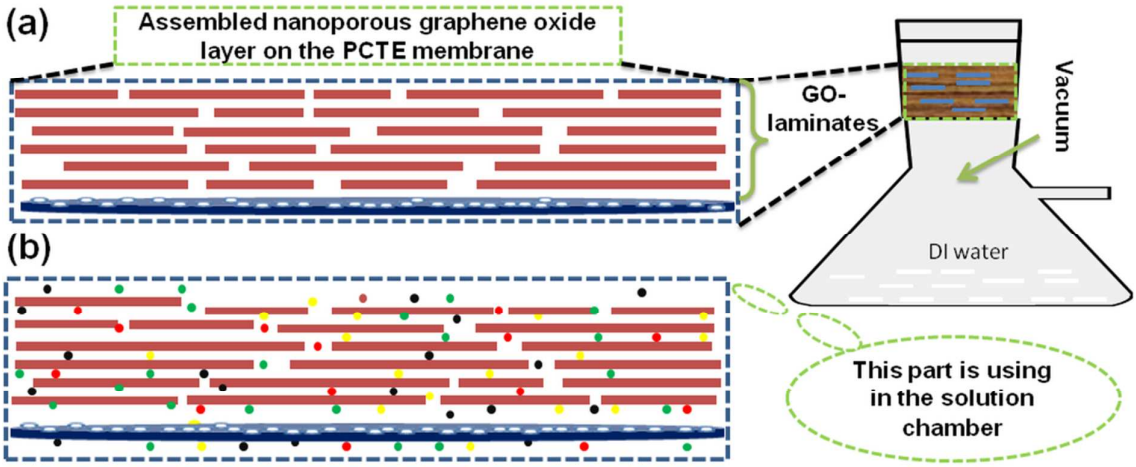

Scheme 3. (a) Main type of randomly assembled nanoporous layers of GO on PCTE membrane. **(b)** Working image of nanoporous GO layers with PCTE membrane in the solution chamber.

Characterizations of GO-PCTE Membrane. Figure 3 (d) demonstrates the schematic diagrams of the trans-GO coated PCTE membrane. The PCTE membrane was coated with 1 mL (CC = 1 mg/mL) of the GO dispersion without centrifugation using a simple filtration method and assented to scrawny spontaneously (as shown in Figure 3d). Due to the non-uniform coating of nanoporous GO sheets, a centrifuge was used to apply a uniform coating of the GO dispersion solution (CC = 0.3

mg/mL) at 10,000 rpm for 3 min (as shown in Figure 3e). Part d and e of Figure 3 show the inverted microscope images (40X) of the non-uniform and uniform coating on the PCTE membrane. The inset in Figure 3e shows that the prepared nanoporous GO has single and few-laminates. Furthermore, conventional part a and b of Figure 3 show FESEM images of the simple PCTE membrane which reveal that the nanopores have excellent consistency on the membrane which was about 0.08 μm in diameter. After this phase, the membrane pore was clearly visible and few bumps were found on the surface of membrane.[61]

The GO laminates were coated onto the PCTE membrane, and the FESEM images demonstrated that they were consistently applied to the surface of the PCTE membrane (Figure 3c). The FESEM image of the GO-laminates-PCTE membrane indicated a well-disappeared nanosize structure, where GO laminates pores became invisible.[61] To confirm the orderly distribution of the GO-laminates on the PCTE membrane, we employed EDX spectroscopy to identify the membrane surface. As shown in Figure 3f, carbon and oxygen are uniformly spread throughout the sample. These results show that the GO laminates were equally attached to the PCTE membrane. This membrane is not conducive to conveniently transporting ions through the laminates, but it has mechanical stability against physical damage due to little increase of the variable pressure in the event.

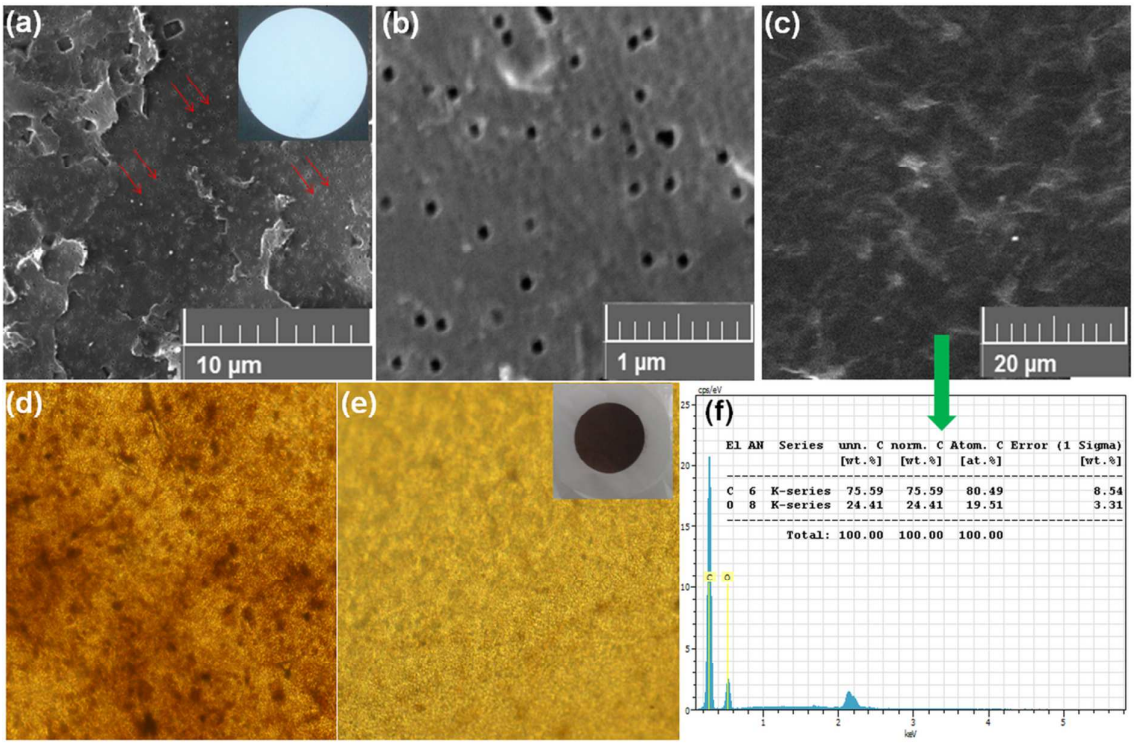

Figure 3. (a,b) FESEM images of the simple PCTE-membrane show the pores at different scales. The red arrow indicates a pore and the inset image shows the simple PCTE-membrane in Figure 3a. **(c)** FESEM images of the GO-laminates on PCTE membrane. **(d)** Non-uniform coating of nanoporous GO sheets on the PCTE membrane. **(e)** Uniform coating of nanoporous GO laminates on the PCTE membrane. **(f)** EDX data of GO laminate-coated PCTE-membrane.

After vacuum filtration of the solution of dispersed GO laminates onto a nanoporous PCTE membrane, morphology of the resulting nanosieve platform is scanned directly using high-resolution AFM imaging. Figure 4a shows an AFM image that exhibits GO laminates from different angles for both the height (Figure 4a) and thickness perspectives (inset Figure 4a). The AFM image (Figure 4a) of the hydrosol endows instantaneous proof for a few layers of GO-coated PCTE membrane; they layers had a maximum thickness of approx 6 nm, indicating the successful exfoliation of each laminates to a few laminates as shown in Inset Figure 4a. As can be seen from Figure 4a, the planar nature of GO

sheets allows them to be in good contact with the flat substrate as well as the stacks of GO layers. All GO are orientated in parallel to the mica and packed firmly into a multi-layer structure. The few layers of GO height we formed are within a very short range of 0 – 99.3 nm, as shown in Figure 4a. Further, the three dimensional image has been captured in the supporting information Figure S5. As discussed in the previously published manuscript in Science,[43] these GO layers should be generally few in number. The GO-layers are small-scale and more 'uneven' than prophesied, which is very likely due to the presence of abundant functional groups, namely epoxy and hydroxyl groups, bonded to both sides of the GO layers, which disorganizes the real conjugation and probably creates lattice shortages that in turn result in folds and distortions in the layers. The observations on AFM (Figure 4a) suggest that most GO layers are of a comparatively large size in the range of several hundred nanometers to tens of micrometers. FESEM characterizations of the cross-section of the GO-laminates coated membranes are shown in Figure 4b, which demonstrate that the as-prepared GO-laminates membrane possesses a lamellar structure. The thickness of PCTE membrane and GO-laminates was less than 3 μm, and few nanometers respectively, as shown in Figure 4b.

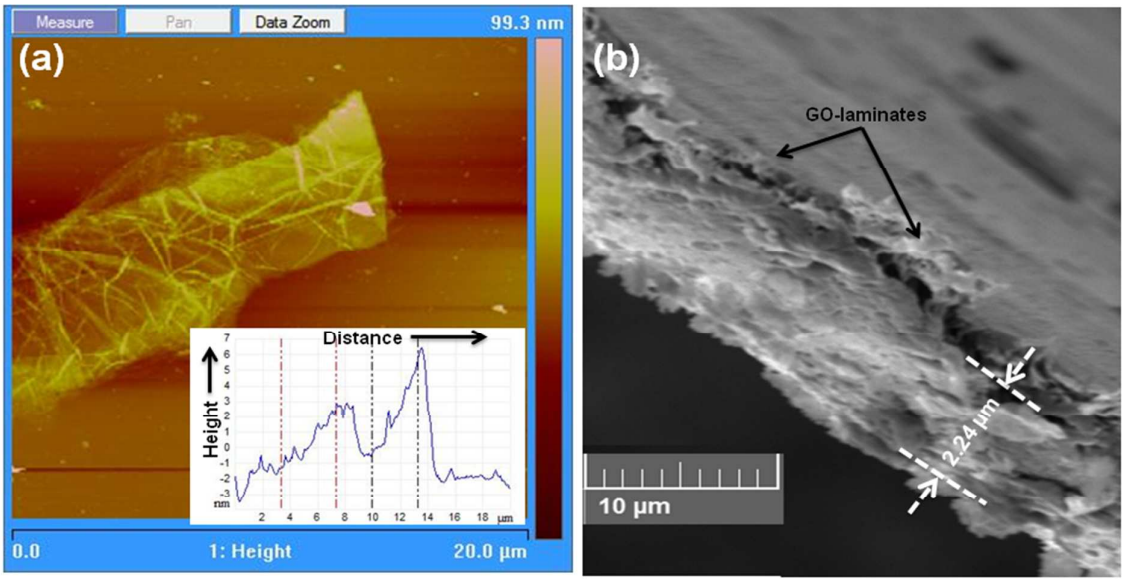

Figure 4. (a) High-resolution AFM imaging of poly-layered GO laminates absorbed on a nanoporous PCTE membrane (scan rate: 1.99 Hz); inset image shows the corresponding AFM height profiles of GO laminates **(b)** Cross-sectional FESEM image of GO-laminates coated PCTE membrane.

Characterizations of Immobilization of 2Dm2m and gp140$_{MS}$ Protein on the GO-PCTE. In this experiment**,** the 2Dm2m protein covers the nanocapillaries of GO laminates and inactivated protein is left by PBS. Figures 5a, b, and c show FESEM images from after the introduction of the 2Dm2m and gp140$_{MS}$ protein on the GO laminates. Figure 5a exhibits interlaminate spacing for probable transport of ions and partial blockage by 2Dm2m protein[47,48] over the GO-laminates. The incubation of 2Dm2m antibody protein is indicated by flamboyant points (shown by the red arrow) on the GO laminates. The protein is connected to the laminates through EDC-NHS interaction as shown in scheme 1.

The functionalized GO laminates were explicated to the augmentation concentration of the gp140$_{MS}$ antigen protein. Each concentration was immobilized on the GO laminates for 30 min at room temperature, transferred into a solution chamber and electrically paraphrased by monitoring the I-V characteristics. Figure 5b and c show the FESEM images of the GO laminate nanosieve platform after being exposed to the gp140$_{MS}$ protein. The gp140$_{MS}$ antigen appears as little bright points around the antibody on the GO laminates.

Additional, to identify EDX data of the antibody, antigen with GO laminates platform, carbon, oxygen and nitrogen element were carried out. The EDX spectra of the 2Dm2m protein *via* EDC-NHS

with GO laminates showed a larger amount of carboxylic groups with the antibody (Figure 5d). The EDX results indicated 75.59 wt% normal carbon and 80.49 wt% atomic carbon as shown in Figure 3f. The 2Dm2m protein with the GO laminate membrane had 62.83 wt% normal carbon, 27.95 wt% oxygen, and 3.62 wt% nitrogen, 70.27 wt% atomic carbon, 23.46 wt% oxygen, and 3.47 wt% nitrogen, as shown in Figure 5d. There was 3.26 wt% normal nitrogen in the $gp140_{MS}$ protein over the nanosieve platform, which was similar to the 2Dm2m protein nanosieve platform (3.62 wt. %), as shown in Figures 5d and e respectively. The atomic oxygen content was as larger in the $gp140_{MS}$ protein GO laminate nanosieve platform (39.37 wt. %) than in the 2Dm2m protein laminates platform (23.46 wt. %).

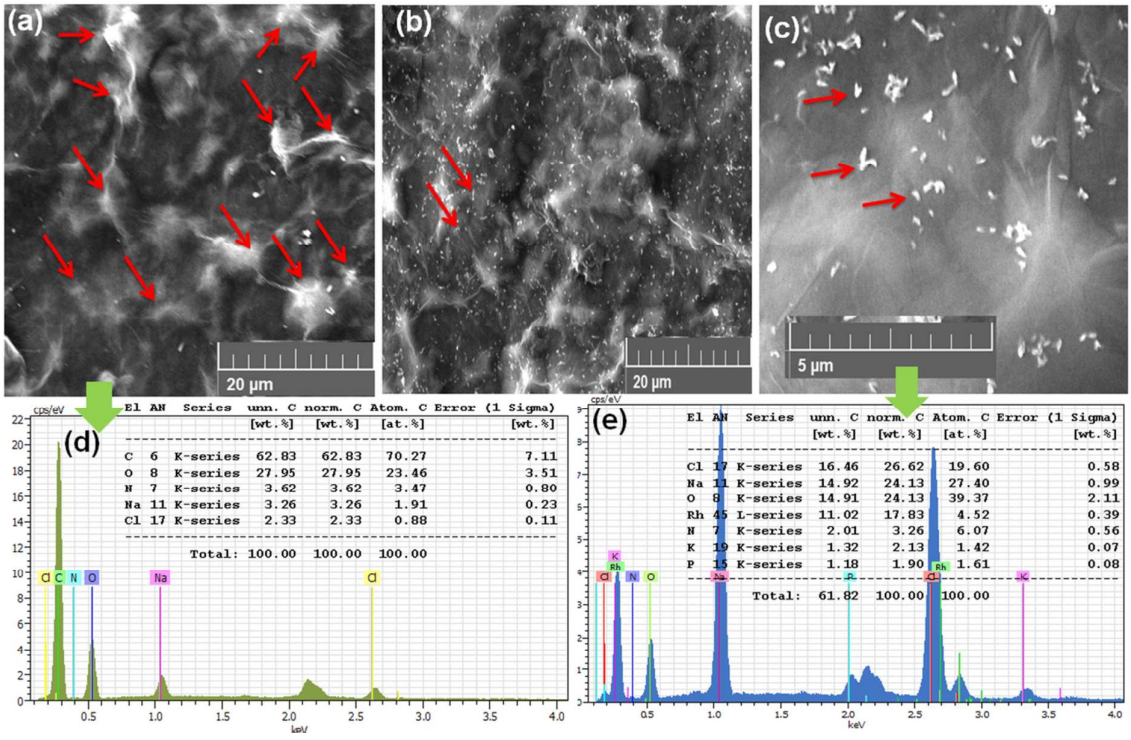

Figure 5. (a) High-magnification FESEM images of 2Dm2m on the GO laminate. Red arrow shows the antibody on the GO laminates. The green arrow indicates a scanning trace of EDX spectra of the 2Dm2m with GO laminates. **(b, c)** FESEM images of $gp140_{MS}$ with 2Dm2m on GO laminates at a different scale. The green arrow indicates a scanning trace in the EDX spectrum of $gp140_{MS}$ with 2Dm2m on GO laminates. **(d)** EDX spectrum of the 2Dm2m with GO laminates. **(e)** EDX spectrum of $gp140_{MS}$ with 2Dm2m on GO laminates.

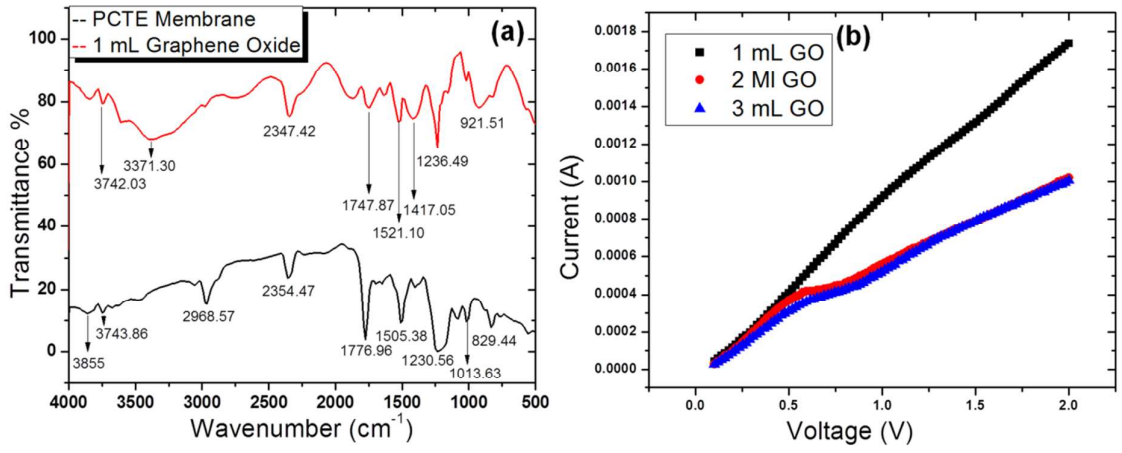

Figure 6. (a) FTIR spectra of the simple PCTE-membrane (black line) and GO-laminate coated PCTE-membrane (red line). **(b)** I-V scattered plot of different GO laminates on PCTE membrane: 1 ml (black line), 2 ml (red line), and 3 ml (blue line).

GO-laminates endure various polar oxygenated functional groups in exclusion of hydroxyl, carbonyl, and carboxyl groups. Its anatomical framework is shown in scheme 2, and FTIR spectra are shown in Figure 1a. Herein, first, these functional groups were noticed in simple polycarbonate membrane and GO-laminates over the polycarbonate membrane by FTIR-simple membrane holder analysis (Figure 6a). The sample scan spectrum demonstrates the occupancy of functional groups of the simple membrane[62] (black line) and GO-laminate coated membrane (red line), such as C–H stretch (aromatic) (~2968.57 cm^{-1}, 2354.47 cm^{-1}), C=O stretch (~1776.96 cm^{-1}), C=C stretch (~1505.38 cm^{-1}), and C–O stretch (~1230.58 cm^{-1})[63] as well as similar to the polycarbonate from bisphenol A polycarbonate, bis(4-hydroxyphenyl)-2-propane.[62,64] Furthermore, Figure 6a clearly shows the difference between the PCTE membrane and the GO-coated membrane. A change near 3000 to 3500 cm^{-1} O-H (~3371.30 cm^{-1}) and an increase in the C=C stretch (~1521.10 cm^{-1}) and C-O-C (~921.51 cm^{-1}) bonds were observed in the GO laminates coated membrane. These functional groups put forward numerous potential for chemical and hydrogen bonds with the EDC-NHS polymer, exceptionally in the matter of large C/O ratio on the GO-laminates (see the EDX data in Figure 3f). Afterward, EDC-NHS, 2Dm2m, and $gp140_{MS}$ proteins were successively immobilized onto the GO-laminates, and some peaks were then shifted from ~ 3371.30 cm^{-1} to ~ 3398.84 cm^{-1} (N-H stretching vibration), ~ 1747.87 cm^{-1} to ~ 1776.14 cm^{-1} (amine), and ~ 1521.10 cm^{-1} to ~ 1505.28 cm^{-1} (amine) in all stepwise functionalization process, while the value of transmittance gets reduced due to the concentrated sample. These results indicated the immense interaction between all groups (protein) with GO-laminates and were further confirmed by FTIR (see the supporting information Figure S6). Furthermore, the new peak 2969.56 cm^{-1} is available due to the symmetric and asymmetric C-H stretching vibrations.[64] The protein molecules hold minimum non-aromatic linear CH-groups as compared to the surface of the GO-laminates. In addition, 2Dm2m antibodies were directly immobilized over the exposed GO-laminates nanosieve platform surface without EDC-NHS and then major peaks were missed in the FTIR spectra (see the supporting information Figure S7) such as ~ 3398.84 cm^{-1} (N-H stretching vibration), 1776.14 cm^{-1} (amine), and 1505.28 cm^{-1} (amine). These peaks play a vital role in the specific binding of antibody with carboxylic groups and some peaks were shifted from ~ 2969.56 cm^{-1} to ~ 2943.71 cm^{-1} with minimum intensity (symmetric and asymmetric C-H stretching vibrations).

Analysis of the Ionic Current Blockade. To better understand the current blockade, it is important to first understand the mechanism of separation of GO laminates immobilised on the PCTE membrane; therefore, we conducted several treatments**.** The crystalline arrangement of the GO laminates was monitored by X-ray diffraction (XRD) over the 2θ range of 0° to 90° in detail. As shown in the inset in Figure 2a, the moistureless GO laminates demonstrate a peak at 2θ = 10.05°, and 42.4°, corresponding to a GO d-spacing of 0.88 nm and 0.21 nm, respectively, which consents well-being with the value previously reported by others manuscript.[31,65] Furthermore, Kang et al. have demonstrated that the GO laminates gaping is in general between 0.6 and 1.0 nm, while it depends on the development method[17] and Chen et al. also demonstrated the 0.747 nm spacing of GO-laminates.[44] This spacing in the GO laminates is larger than the ionic radius (diameter) of used ions (salts) in PBS solution, as shown in Table 1. These results show that sieving properties may have provided well-being to the motion of ions through GO laminates.

An order of ion-penetration measurements was performed with a homemade glass chamber separated by the GO laminated coated PCTE membrane (as shown in the supporting information Figure S8). The entire discriminating ion-penetration characteristic was first acquired from the different volume GO suspension coating on PCTE membrane and the current was monitored using ion penetration through the GO-laminates, as shown in Figure 6b. The current of all GO-laminates with a concentration of 0.3 mg/mL were in the range 0.0017-0.0010 A, whereas the current of all GO-laminates were on the series of A. The current of some of the penetration ions changed their volume coating of

GO laminates on PCTE membrane. As shown in Figure 6b, the currents of all 0.3 mg/mL (different volume *i.e.,* 2mL, and 3mL) GO-laminates showed similar tendencies, while 1 mL GO-laminates exhibited different tendencies compare to the 2 mL and 3 mL. Because ions easily penetrate through the GO-laminates in 1 mL coating, the current was increased. In the primary level, the current changed slightly, whereas it increased considerably in a near-linear mode subsequently. All salts permeated without difficulty through the GO-laminates (1 mL), whereas these salts filtrated much more slowly in 2 mL and 3mL coated GO-laminates membrane, which is highly coated GO-laminates. Lastly, we used 1 mL coated GO-laminates on a PCTE membrane for sensing.

However, we first introduce the output acquired with 2Dm2m proteins. Successive addition of 2Dm2m proteins via EDC-NHS on the GO laminates for two hours in the wet condition easily removed extra 2Dm2m protein by the PBS, which is not attached to the linker molecules (EDC-NHS). Then it was placed in the negative (*cis*) chamber, and deep ionic current blockades were noticed (Figure 7a). Details of the blockade ionic current are shown in Figure 7a. The reference level of the ionic current remains identical parallel to acquisition activity, frequently conducted for several minutes. In Figure 7a, we observed short rectangular events corresponding to a single protein over the laminates of GO. This figure assents us to explain the principal characteristic of the ionic current monitor: blockade period T_t, related to reside of a protein over the laminates; inter-event time T_i, related to the time of blockades; open laminates ionic current I_o (associated with the laminates conductance); and average blockade laminates ionic current with 2Dm2m I_b (Figure 7a). Figure 7a shows a plot of the ionic current blockade = I_o-I_b (i.e., 0.233 mA) vs the T_t exhibiting the classical correlation between the deep blockades. We have orderly analyzed the ionic current variation A *versus* applied voltages (Figure 7b). We concluded that the applied voltage and ionic current variation of the $gp140_{MS}$ protein (Figure 8a) are larger than those of the 2Dm2m protein. The ionic current blockade could be modulated with the odds in an occupied volume of the laminates' spacing by the 2Dm2m and combined with $gp140_{MS}$ protein. Further, we observe the action of GO laminates of the 2Dm2m and corresponding $gp140_{MS}$ proteins in terms of ion motion through GO-laminates, electrostatics force of attraction, and drag force. We checked the blockades ionic current (Figure 7a) from the complete ionic current analysis shown in Figure 7b. Herein, we checked two different conditions: the first corresponds to the noise ionic current of the "open GO-laminates spacing", and the second corresponds occupancy of the 2Dm2m and with $gp140_{MS}$ proteins over the GO-laminates (Figure 7b, 8a, b). We equate, in Figure 8a, b, the blocking ratio of 2Dm2m and with $gp140_{MS}$ proteins. The blockade ionic current is defined as $(I_o\text{-}I_b)/I_o$ and the percentage of the blockade ionic the current as $(I_o\text{-}I_b)/I_o$ x 100 as shown in Figure 8b; we analyze that ionic current is not dependent on the voltage for 2Dm2m and with $gp140_{MS}$ proteins. These results convey that the blockades are surely due to the existence of the proteins over the laminates' spacing. This event was also noticed when we immobilized the non-corresponding antigen (BSA) (data not showed) with different concentrations. The ionic current was not changed with different concentration of BSA antigen as the same applied voltage as such 0.1V to 2V. This means that the confirmation of the detection to the 2Dm2m and with $gp140_{MS}$ protein. In addition, this event suggests offers that the volume is filled by the 2Dm2m and with $gp140_{MS}$ protein in the GO-laminates and that ionic current decrease as the voltage increases. All of these mental analyses allow us to assume that 2Dm2m and with $gp140_{MS}$ protein created the resistance as the applied voltage increases. We prepare an additional significant analysis by correlating the value of blockades ionic current with 2Dm2m, $gp140_{MS}$ protein, $I_B = (I_o\text{-}I_b)/I_o$, to its principled value, which is to a first closeness the volume occupied by the protein over the laminates. For the 2Dm2m protein acceded to be pyramid $V_{2Dm2m}/V_{laminate\ spacing} = (1/3bc)/(\pi r^2_{laminates}\ L_{laminates})$, with a, b, and c being the 2Dm2m dimensions 18, 6, and 12 nm, respectively, and by considering a cylindrical laminates shape of radius $r_{laminates}$ and length $L_{laminates,}$ $V_{2Dm2m}/V_{laminate\ spacing}$ = 3.7 %, we acquired $I_B = (I_o - I_b)/I_o$ = 10.19 $\pm$ 1.58% (Figure 7b). Both values are much closer when three or four antibodies were immobilised over the laminates of GO.

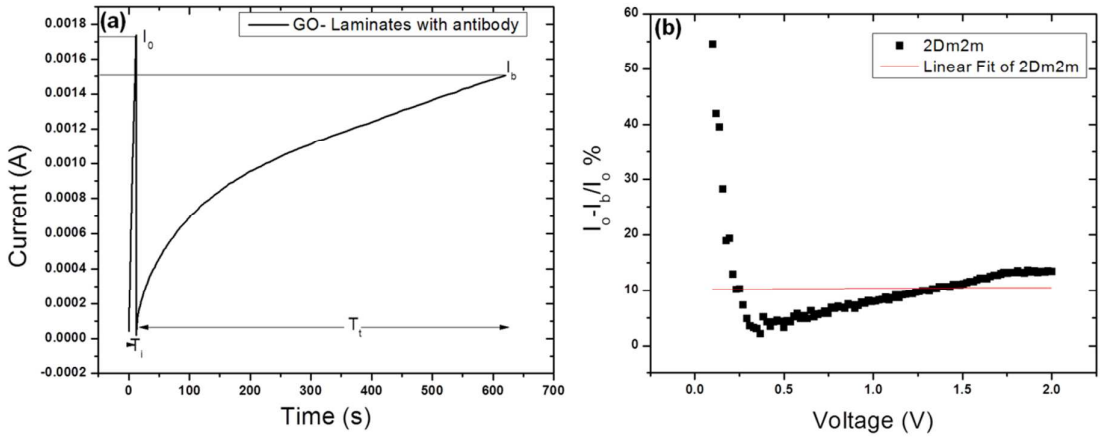

Figure 7. (a) This graph shows two consecutive distinctive events, with corresponding blockades time T_t, inter-event time T_i, ionic current scale of the empty laminate spacing I_o, blockade laminate ionic current I_b, and ionic current blockade = 0.000233 A. This 2Dm2m protein concentration is 0.3 μM. **(b)** The progress of the blockade ratio is (%) $(I_o\text{-}I_b/I_o)$ x100 according to the applied voltage. The red line is the linear fit of the equation f(V) = bV + a. We acquire a = 10.19 ± 1.58%, b = 0.178 ± 1.33% V^{-1} for the 2Dm2m protein.

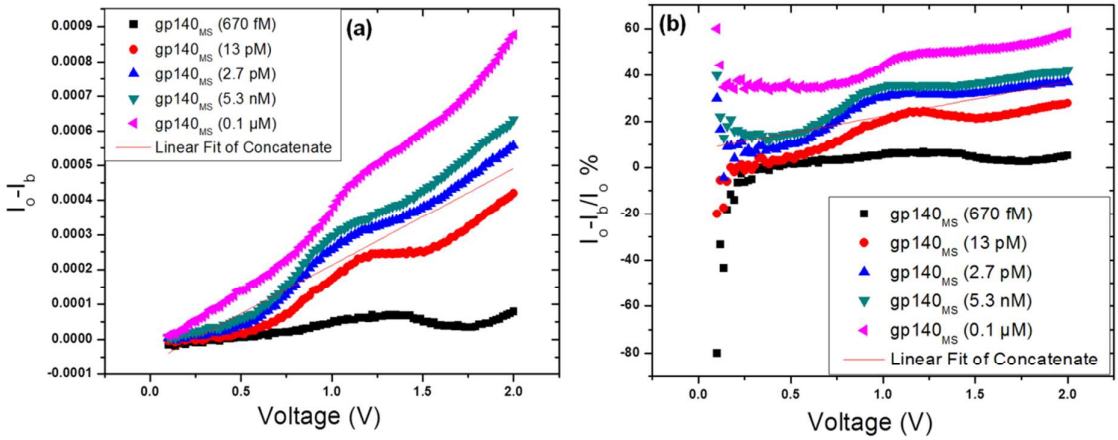

Figure 8. (a) Evolution of the ionic current blockade $I_o - I_b$ according to the applied voltage for MS140 (antigen). The red line is a linear fit whose equation is f(V) = bV + a, with a = - 6.64 e^{-5} ± 1.3 e^{-5} A, b = 2.78 e^{-4} ± 1.17 e^{-5} AV^{-1}. **(b)** The ionic blockade ratio is (%) $(I_o - I_b)/I_o$ x 100 according to the applied voltage. Herein, the red line is shown as the linear fit equation f(V) = bV + a. We acquired a = 7.77 ± 1.50%, b = 14.61 ± 1.26% V^{-1} for $gp140_{MS}$ protein.

Later, we show that the ionic blockade current of the $gp140_{MS}$ protein attaches to the 2Dm2m protein on the GO laminates (Figure 8a, b). First, we immobilised different concentrations of $gp140_{MS}$ protein such as 670 fM, 13 pM, 2.7 pM, 5.3 nM, and 0.1 μM onto the 2Dm2m protein GO laminates. Subsequently, each concentration was immobilised onto the 2Dm2m GO laminates, and each concentration was eliminated by the PBS, which is not attached to the 2Dm2m protein. For the 2Dm2m with $gp140_{MS}$ protein acceded to be pyramid $V_{2Dm2m\text{-}gp140MS}/V_{laminate\ spacing} = (1/3BC)/(\pi r^2_{laminates}\ L_{laminates})$, with a, b, and c being the $gp140_{MS}$ dimensions 5, 6, and 11 nm and with A, B, and C being 2Dm2m with $gp140_{MS}$ dimensions 18, 6, and 23 respectively, and by considering a cylindrical laminates shape of radius $r_{laminates}$ and length $L_{laminates}$, $V_{2Dm2m\text{-}gp140MS}/V_{laminate\ spacing}$ = 3.32 %, we acquired $I_B = (I_o - I_b)/I_o$ = 7.77 ± 1.50% (Figure 8b). These result are in an agreement with the practical value of the normalized current blockade ratio $[(I_0\text{-}I_b)/I_0]$ at the stage (7.77 ± 1.50%).[66,67] Both values are much closer when three or four antigens immobilized over the laminates of GO. The hypothetical appraise allows the correct order of quantity of the notice values. Thus, we draw a conclusion from the difference between

both values that the ions are a little hindrance to the protein under the applied voltages, as shown in scheme 4. Furthermore, this fabricated nanosieve platform have also analyzed (see the supporting information Figure S9 and S10) by four HIV positive and two negative human serum samples (see the supporting information Figure S1). We observe that the blockades ionic current increases as a function of the applied voltage from 0.1 to 2 V (Figure S9 and S10) for different concentration of using human serum (that is 2Dm2m, HIV-infected human serum). We equate, in the supporting information Figure S9a, b, the blocking ratio of 2Dm2m and with HIV human serum samples. These results convey that the blockades are surely due to the existence of the proteins and human serum samples with different concentrations over the laminates' spacing. This event was also noticed when we immobilized the negative human serum first sample (74.75 g/L) and second sample (77.86 g/L) (not infected HIV) (data showed in the supporting information Figure S10). The ionic current was changed with different concentration of HIV-infected human serum (see the supporting information Figure S9) as the same applied voltage as such 0.1V to 2V. However, the first (46.25 g/L) and third positive (75.92 g/L) sample of HIV showed the minimum change in the blockade ionic current and showed the maximum blockade ionic current in the second (46.17 g/L) and fourth samples (60.83 g/L). The ionic current did not change with negative human serum samples (same as 2Dm2m protein shown in the supporting information Figure S10) at the same applied voltage as 0.1V to 2V, confirm the presence of HIV in these human sera. An in-house fabricated glass cell (see the supporting information Figure S11) was used for the measurements of ion trafficking with protein and real samples. It is evident from Figures S9 and S10 that our GO-laminate nanosieve platform successfully confirms the detection of HIV in real samples; however the variation in respect of total protein concentration during the detection may be a transient post-treatment effect on unknown patients, which may be a part of further study. These results seem in good accordance with the results of commercial methods (Western Blot, enzyme-linked immunosorbent assay and rapid diagnostic tests) employed for these real samples.

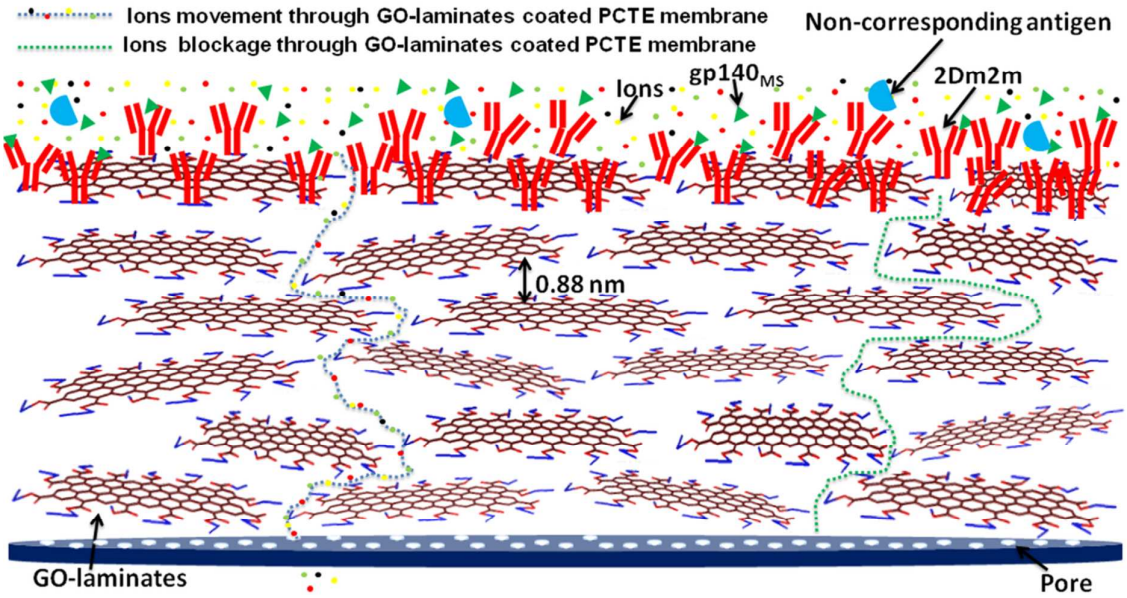

Scheme 4. The depicted diagram shows the ions mediate through the GO-laminates with and without the antigen-antibody.

Analytical Accomplishment of the Nano-Biosensor. The analytical fulfilments of this nano-biosensor were estimated through the response time, sensitivity, and detection limit, as shown in Figure 9. The response of fluidic electrochemical biosensor is shown in Figure 9a. In this graph, five readings were noticed gradually for 60 sec to learning the progression of the present biosensor for each of the $gp140_{MS}$ concentrations. In addition, this platform demonstrated a quick response, attain-

ing the 88% of the regular-state ionic current within the 12 s. Further, the measurement line was provided as a function of $gp140_{MS}$ concentration, as shown in Figure 9b. At immense levels of $gp140_{MS}$ protein (*i.e.,* 670 fM to 0.1 μM), this linear curve was fit with $y = - 1.39771e^{-4} x - 3.47446e^{-4}$, where y is the ionic current and x is $gp140_{MS}$ concentration, and the linear regression $R^2 = 0.92741$ and slope m = 0.13977 $mAmM^{-1}$ were as well acquired. The measurement curve demonstrates a linear relationship between the maximum current value and $gp140_{MS}$ protein concentration. As a result, the sensitivity of this biosensor computed was 0.87mA-$mM^{-1}cm^{-2}$ at the active electrode sensing surface area, 0.16 cm^{-2} and using this formula sensitivity = slope of the measurement curve/active electrode surface area.

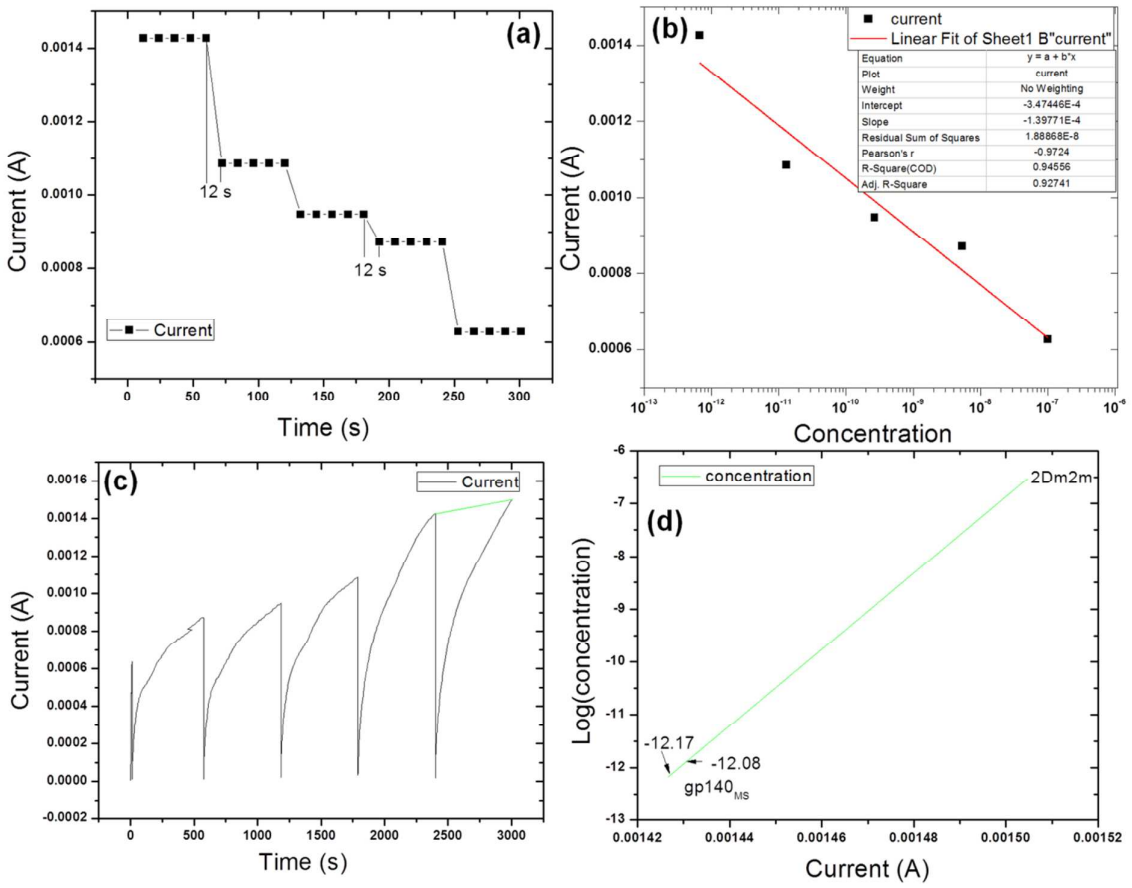

Figure 9. Examination and determination of response time, sensitivity, and detection limit of reference $gp140_{MS}$ detection. **(a)** The electro-analytical measurement curve for every concentration calculated at 12 s with the linear regression, as shown in the Figure **9b**. **(c)** The amperometric measurement curve was drawn, and the limit of detection measured from Figure **9d** is 8.3 fM.

However, the amperometric reaction was as well examined and determined to get the limit of detection of this biosensor (Figure 9c, d). We notice that the maximum ionic current for corresponding $gp140_{MS}$ concentration was elongated from 670 fM to 0.1 μM. At 670 fM, the current began to saturate and the given point was fluctuated to the detection limit. For calculating the detection limit, the graph of maximum current of 670 fM and immobilized 2Dm2m/EDC-NHS/GO-laminates were drawn (in green line) *vs* current (Figure 9d). Due to this observation, the detection limit was measured (8.3 fM), which was acquired at 1.42 mA from log^{-1} (-12.08) (Figure 9d) and as well measured using enzyme-linked immunosorbent assay, which presents the minimum limit at 50ng (Figure 10a).

Development of Experimental Stage. To calibrate the optimum biosensor stages, we renovated two experimental aspects. On account of the concentration of incarcerate $gp140_{MS}$ protein is of very large significance for selecting the tremendous signal change in percentage $(I_o - I_b)/I_b$, six different

concentration of $gp140_{MS}$ (from 670 fM to 0.1 μM), and five different BSA concentration (from 150 pM to 0.15 μM) were used to check the optimal situation (data showed only single concentration of BSA in Figure 10c). We observe that the blockades ionic current increases constantly as a function of the applied voltage from 0.1 to 2 V (Figure 10b) for different concentration of using protein (i.e., 2Dm2m, $gp140_{MS}$). When the incarcerate $gp140_{MS}$ protein increased from 670 fM to 0.1 μM, the ionic current change percentage decreased because more incarcerate $gp140_{MS}$ protein had been immobilised on the platform. In contrast, a continuous increase the incarcerate protein from 670 fM to 0.1 μM led to a ionic current percentage change decrease of each concentration of $gp140_{MS}$ and minimum current percentage change in 670 fM concentration of $gp140_{MS}$ with 2Dm2m protein (Figure 10b). Hence, we selected 670 fM as the excellent concentration to establish this proposed biosensor. The incubation time of the $gp140_{MS}$ had very well effect on the 2Dm2m with EDC-NHS over the GO-laminates, while it did not substantially affect the recycling process. To examine the good incubation time, $gp140_{MS}$ was added onto the 2Dm2m antibody and incubated at 25°C for different concentrations.

Selectivity, Reproducibility, and Stability of the Biosensor. Selectivity and reproducibility of the proposed biosensor were examined through intervention observations and revised monitoring. Six types of antigen sequences five complete matched sequences of 2Dm2m with different concentration and one-base mismatched of 2Dm2m were identified under the alike limitation, respectively, for precision detection with the intervention $gp140_{MS}$'s different concentration greater than unmatched target BSA. As shown in Figure 10c, insignificant enzyme-linked immunosorbent assay results were noticed with the addition of interloping $gp140_{MS}$ compared with the increase of the electrochemical signal due to target sequencing, which revealed the proposed biosensor had large specificity to the target $gp140_{MS}$ detection for the cause that effect of 2Dm2m/EDC-NHS/GO-laminates good activity provided the superior selectivity of the developed biosensor. Herein, four different platforms were demonstrated to identify $gp140_{MS}$ target protein (0.1 μM) and two times under the same condition (Figure 10d) to analysis the reproducibility of the proposed biosensor. The present biosensor showed similar decreases, where 0.877378, 0.877382, 0.877380, and 0.877380 mA was accumulated; as well the collected relative standard deviation (RSD) was below 0.141%. These results signified that the developed biosensor has excellent reproducibility.

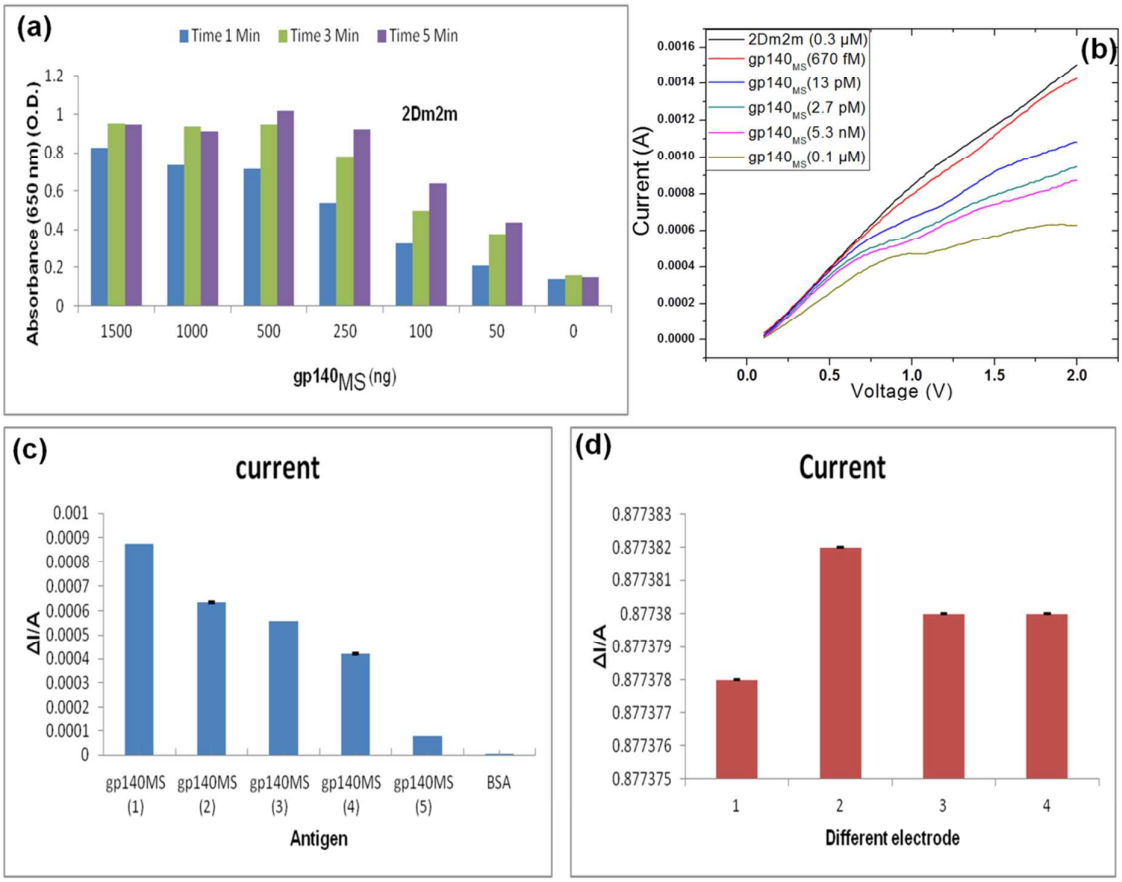

Figure 10. (a) The detection limit was as well measured using enzyme-linked immunosorbent assay, which presents the minimum limit at 50ng. **(b)** The variation of current in different concentration of $gp140_{MS}$ against voltage. **(c)** Selectivity analysis of the present biosensor for (1) HIV target $gp140_{MS}$ (0.1 μM), (2) HIV target $gp140_{MS}$ (5.3 nM), (3) HIV target $gp140_{MS}$ (2.7 pM), (4) HIV target $gp140_{MS}$ (13 pM), (5) HIV target $gp140_{MS}$ (670 fM), and (6) Unmatched target BSA concentration 0.15 μM to 150 pM. **(d)** The reproducibility of this biosensor for detection of a target with four different platforms under the optimal conditions with 670 fM target.

Table: 1 Show the ionic diameter of using salts in PBS solution.

Use Ions	Ionic weight (Da)	Ionic radius (nm)	Ionic Diameter (nm)	References
Na^+	23.0	0.098, 0.101, 0.102, 0.116, 0.117	0.196, 0.202, 0.204, 0.232, 0.234	68
K^+	39.0	0.133, 0.138, 0.149, 0.152	0.266, 0.276, 0.298, 0.304	68
Cl^-	35.5	0.167, 0.181, 0.194	0.334, 0.362, 0.388	68
PO_4^{-3}	95.0	0.223, 0.238	0.446, 0.476	68

Table: 2 Comparison between recently published papers for HIV detection

Modification biosensor platforms	Biosensor	Dynamic range	Detection limit	References
Graphene stabilized gold nanoclusters	Electrochemical bio-sensor	0.1 fM – 100 nM	30 aM	69
mAbs A32 or T8 immobilized microcantilever surface *via* polyethylene glycol	Microcantilever de-flection biosensor	8 $\mu g.mL^{-1}$ gp120 and 0.17 $mg.mL^{-1}$ 17b	Less than 400 $ng.mL^{-1}$	45
Gold nanoparticle modified ITO electrode	Electrochemical bio-sensor	600 $fg.mL^{-1}$ – 375 $pg.mL^{-1}$	-	46
Graphene oxide laminates on	Two electrode elec-	670 fM - 0.1 μM	8.3 fM	This work

the PCTE membrane/EDC-NHS/2Dm2m	trochemical biosensor

CONCLUSION

In summary, a novel and impressionable two-electrode ECB was established for $gp140_{MS}$ detection based on a PCTE membrane modified with GO-laminates and a receptor 2Dm2m protein. This manuscript demonstrated the selective ions penetration properties of GO-laminates *via* a simple filtration method. The made whole GO laminates nanosieve platform with homogeneous allocation was characterized by the FESEM, FTIR and XRD, UV-Vis. This nanocomposite is an excellent biosensing nanosieve platform with immense activator ability for the discrimination and sensitive a foregone detection towards the $gp140_{MS}$ protein accomplished other interfering non-corresponding protein (*i.e.,* BSA) with 2Dm2m protein plan of action in our work. Besides, by taking advantage of the 2Dm2m protein bind via EDC-NHS on the GO-laminates, we acquired excellent electrochemical results for the $gp140_{MS}$ protein. Finally, our detection limit, sensitivity, and response time for $gp140_{MS}$ protein are 8.3 fM, 0.87 mA-$mM^{-1}cm^{-1}$ and 12 s respectively, which allows for the immediate detection of HIV samples. The successful testing of platform with real samples bestowed the concept and experimental evidence of proposed new nanosieve device. This research work is important for medical diagnostics or other applications. Also proposed nanobiosensor has excellent potential for the sensitive evaluation of other analytes corresponding to antibodies, in terms of small biomolecules.

ASSOCIATED CONTENT

Supporting Information

This part includes additional material (Figure S1-S11) related to the synthesis of few layered GO, spectrophotometric determination of concentration of GO, picture of in-house fabricated special glass cell used, Developed GO-PCTE nanosieve platform, IR depiction of functionalization of nanosieve, three dimensional image of GO-laminates, I-V graph of human serum sample, human serum sample image, and positive & negative human serum sample detection experiments. This material is available free of charge *via* the Internet at http://pubs.acs.org.

AUTHOR INFORMATION

Corresponding Author

*E-mail: kps_biophysics@yahoo.co.in. (Krishna Pal Singh)

ORCID

Krishna Pal Singh: org/0000-0002-2062-4764

Notes

The authors declare no competing financial interest.

ACKNOWLEDGMENTs

Authors acknowledge the financial assistance provided by Indian Council of Medical Research (ICMR) and Department of Biotechnology (DBT), government of India and NCI/NIH (Frederick, USA) under I-to-I Grant of Indo-US project via its project sanction no. BT/MB/Indo-US/BCRP/01/2012 dated 30/07/2012. This work was also supported by the Intramural Research Program of the NIH, National Cancer Institute, Center for Cancer Research.

REFERENCES

(1) Nehra, A.; Singh, K. P. Current Trends in Nanomaterial Embedded Field Effect Transistor-Based Biosensor. *Biosens. Bioelectron.* **2015**, *74*, 731–743.

(2) Lee, G. H.; Yu, Y.; Cui, X.; Petrone, N.; Lee, C. H.; Choi, M. S.; Lee, D. Y.; Lee, C.; Yoo, W. J.; Watanabe, K.; Taniguchi, T.; Nuckolls, C.; Kim, P.; Hone, J. Flexible and Transparent MoS_2 Field-Effect Transistors on Hexagonal Boron Nitride-Graphene Heterostructures. *ACS Nano* **2013**, *7* (9), 7931–7936.

(3) Rao, A.; Long, H.; Trochimczyk, A. H.; Pham, T.; Zettl, A.; Carraro, C.; Maboudian, R. In Situ Localized Growth of Ordered Metal Oxide Hollow Sphere Array on Microheater Platform for Sensitive, Ultra-Fast Gas Sensing. *ACS Appl. Mater. Interfaces* **2017**, 9 (3), 2634–2641.

(4) Tan, C.; Zhang, H. Wet-Chemical Synthesis and Applications of Non-Layer Structured Two-Dimensional Nanomaterials. *Nat. Commun.* **2015**, *6*, 7873.

(5) Tung, T. T.; Yoo, J.; Alotaibi, F. K.; Nine, M. J.; Karunagaran, R.; Krebsz, M.; Nguyen, G. T.; Tran, D. N. H.; Feller, J. F.; Losic, D. Graphene Oxide-Assisted Liquid Phase Exfoliation of Graphite into Graphene for Highly Conductive Film and Electromechanical Sensors. *ACS Appl. Mater. Interfaces* **2016**, *8* (25), 16521–16532.

(6) Zhu, Y.; Murali, S.; Cai, W.; Li, X.; Suk, J. W.; Potts, J. R.; Ruoff, R. S. Graphene and Graphene Oxide: Synthesis, Properties, and Applications. *Adv. Mater.* **2010**, *22* (35), 3906–3924.

(7) Nehra, A.; Pandey, K.; Singh, K. P.; Ahalawat, S.; Joshi, R. P. Determination of *E. Coli* by a Graphene Oxide-Modified Quartz Crystal Microbalance. *Anal. Lett.* **2017**, 1-15.

(8) Huang, H.; Song, Z.; Wei, N.; Shi, L.; Mao, Y.; Ying, Y.; Sun, L.; Xu, Z.; Peng, X. Ultrafast Viscous Water Flow through Nanostrand-Channelled Graphene Oxide Membranes. *Nat. Commun.* **2013**, *4*, 2979.

(9) Abraham, J.; Vasu, K. S.; Williams, C. D.; Gopinadhan, K.; Su, Y.; Cherian, C. T.; Dix, J.; Prestat, E.; Haigh, S. J.; Grigorieva, I. V.; Carbone, P.; Geim, A. K.; Nair, R. R. Tunable Sieving of Ions Using Graphene Oxide Membranes. *Nat. Nanotechnol.* **2017**, *12* (6), 546–550.

(10) Jiang, Z. J.; Jiang, Z.; Tian, X.; Luo, L.; Liu, M. Sulfonated Holey Graphene Oxide (SHGO) Filled Sulfonated Poly(ether Ether Ketone) Membrane: The Role of Holes in the SHGO in Improving Its Performance as Proton Exchange Membrane for Direct Methanol Fuel Cells. *ACS Appl. Mater. Interfaces* **2017**, *9* (23), 20046–20056.

(11) Zhao, Q.; Zhou, Y.; Li, Y.; Gu, W.; Zhang, Q.; Liu, J. Luminescent Iridium (III) Complex Labeled DNA for Graphene Oxide-Based Biosensors. *Anal. Chem.* **2016**, *88* (3), 1892–1899.

(12) Kang, T. W.; Jeon, S. J.; Kim, H. I.; Park, J. H.; Yim, D.; Lee, H. R.; Ju, J. M.; Kim, M. J.; Kim, J. H. Optical Detection of Enzymatic Activity and Inhibitors on Non-Covalently Functionalized Fluorescent Graphene Oxide. *ACS Nano* **2016**, *10* (5), 5346–5353.

(13) Huang, H.; Mao, Y.; Ying, Y.; Liu, Y.; Sun, L.; Peng, X. Salt Concentration, pH and Pressure Controlled Separation of Small Molecules through Lamellar Graphene Oxide Membranes. *Chem. Commun. (Cambridge, U. K.).* **2013**, *49* (53), 5963–5965.

(14) Nellore, B. P. V.; Kanchanapally, R.; Pedraza, F.; Sinha, S. S.; Pramanik, A.; Hamme, A. T.; Arslan, Z.; Sardar, D.; Ray, P. C. Bio-Conjugated CNT-Bridged 3D Porous Graphene Oxide Membrane for Highly Efficient Disinfection of Pathogenic Bacteria and Removal of Toxic Metals from Water. *ACS Appl. Mater. Interfaces* **2015**, *7* (34), 19210–19218.

(15) Liu, Y. Q.; Zhang, Y. L.; Fu, X. Y.; Sun, H. B. Bioinspired Underwater Superoleophobic Membrane Based on a Graphene Oxide Coated Wire Mesh for Efficient Oil/Water Separation. *ACS Appl. Mater. Interfaces* **2015**, *7* (37), 20930–20936.

(16) Wu, W.; Li, Y.; Chen, P.; Liu, J.; Wang, J.; Zhang, H. Constructing Ionic Liquid-Filled Proton Transfer Channels within Nanocomposite Membrane by Using Functionalized Graphene Oxide. *ACS Appl. Mater. Interfaces* **2016**, *8* (1), 588–599.

(17) Huang, K.; Liu, G.; Lou, Y.; Dong, Z.; Shen, J.; Jin, W. A Graphene Oxide Membrane with Highly Selective Molecular Separation of Aqueous Organic Solution. *Angew. Chem., Int. Ed.* **2014**, *53* (27), 6929–6932.

(18) You, Y.; Sahajwalla, V.; Yoshimura, M.; Joshi, R. K. Graphene and Graphene Oxide for Desalination. *Nanoscale* **2016**, *8* (1), 117–119.

(19) Yoon, K. Y.; An, S. J.; Chen, Y.; Lee, J. H.; Bryant, S. L.; Ruoff, R. S.; Huh, C.; Johnston, K. P. Graphene Oxide Nanoplatelet Dispersions in Concentrated NaCl and Stabilization of Oil/water Emulsions. *J. Colloid Interface Sci.* **2013**, *403*, 1–6.

(20) Yeh, T.; Wang, Z.; Mahajan, D.; Hsiao, B. S.; Chu, B. High Flux Ethanol Dehydration Using Nanofibrous Membranes Containing Graphene Oxide Barrier Layers. *J. Mater. Chem. A* **2013**, *1* (41), 12998.

(21) Kim, H. W.; Yoon, H. W.; Yoon, S. M.; Yoo, B. M.; Ahn, B. K.; Cho, Y. H.; Shin, H. J.; Yang, H.; Paik, U.; Kwon, S.; Choi, J. Y.; Park, H. B. Selective Gas Transport Through Few-Layered Graphene and Graphene Oxide Membranes. *Science* **2013**, *342* (6154), 91–95.

(22) Li, H.; Song, Z.; Zhang, X.; Huang, Y.; Li, S.; Mao, Y.; Ploehn, H. J.; Bao, Y.; Yu, M. Ultrathin, Molecular-Sieving Graphene Oxide Membranes for Selective Hydrogen Separation. *Science* **2013**, *342* (6154), 95–98.

(23) Shen, J.; Liu, G.; Huang, K.; Jin, W.; Lee, K. R.; Xu, N. Membranes with Fast and Selective Gas-Transport Channels of Laminar Graphene Oxide for Efficient CO_2 Capture. *Angew. Chem., Int. Ed. Engl.* **2015**, *54* (2), 578–582.

(24) Shen, J.; Liu, G.; Huang, K.; Chu, Z.; Jin, W.; Xu, N. Subnanometer Two-Dimensional Graphene Oxide Channels for Ultrafast Gas Sieving. *ACS Nano* **2016**, *10* (3), 3398–3409.

(25) Wang, W.; Eftekhari, E.; Zhu, G.; Zhang, X.; Yan, Z.; Li, Q. Graphene Oxide Membranes with Tunable Permeability due to Embedded Carbon Dots. *Chem. Commun. (Cambridge, U. K.)* **2014**, *50* (86), 13089–13092.

(26) Zhao, X.; Su, Y.; Liu, Y.; Li, Y.; Jiang, Z. Free-Standing Graphene Oxide-Palygorskite Nanohybrid Membrane for Oil/Water Separation. *ACS Appl. Mater. Interfaces* **2016**, *8* (12), 8247–8256.

(27) Wang, J.; Zhang, P.; Liang, B.; Liu, Y.; Xu, T.; Wang, L.; Cao, B.; Pan, K. Graphene Oxide as an Effective Barrier on a Porous Nanofibrous Membrane for Water Treatment. *ACS Appl. Mater. Interfaces* **2016**, *8* (9), 6211–6218.

(28) Zhao, J.; Zhu, Y.; He, G.; Xing, R.; Pan, F.; Jiang, Z.; Zhang, P.; Cao, X.; Wang, B. Incorporating Zwitterionic Graphene Oxides into Sodium Alginate Membrane for Efficient Water/Alcohol Separation. *ACS Appl. Mater. Interfaces* **2016**, *8* (3), 2097–2103.

(29) Joshi, R. K.; Carbone, P.; Wang, F. C.; Kravets, V. G.; Su, Y.; Grigorieva, I. V.; Wu, H. A.; Geim, A. K.; Nair, R. R. Precise and Ultrafast Molecular Sieving Through Graphene Oxide Membranes. *Science* **2014**, *343* (6172), 752–754.

(30) Sun, P.; Zheng, F.; Zhu, M.; Song, Z.; Wang, K.; Zhong, M.; Wu, D.; Little, R. B.; Xu, Z.; Zhu, H. Selective Trans-Membrane Transport of Alkali and Alkaline Earth Cations through Graphene Oxide Membranes Based on Cation−π Interactions. *ACS Nano* **2014**, *8* (1), 850–859.

(31) Sun, P.; Zhu, M.; Wang, K.; Zhong, M.; Wei, J.; Wu, D.; Xu, Z.; Zhu, H. Selective Ion Penetration of Graphene Oxide Membranes. *ACS Nano* **2013**, *7* (1), 428–437.

(32) Xu, X. L.; Lin, F. W.; Du, Y.; Zhang, X.; Wu, J.; Xu, Z. K. Graphene Oxide Nanofiltration Membranes Stabilized by Cationic Porphyrin for High Salt Rejection. *ACS Appl. Mater. Interfaces* **2016**, *8* (20), 12588–12593.

(33) Yoon, H. W.; Cho, Y. H.; Park, H. B. Graphene-Based Membranes: Status and Prospects. *Philos. Trans. R. Soc., A* **2016**, *374* (2060), 20150024.

(34) Lindsay, S. The Promises and Challenges of Solid-State Sequencing. *Nat. Nanotechnol.* **2016**, *11* (2), 109–111.

(35) Garaj, S.; Hubbard, W.; Reina, A.; Kong, J.; Branton, D.; Golovchenko, J. A. Graphene as a Subnanometre Trans-Electrode Membrane. *Nature* **2010**, *467* (7312), 190–193.

(36) Heerema, S. J.; Dekker, C. Graphene Nanodevices for DNA Sequencing. *Nat. Nanotechnol.* **2016**, *11* (2), 127–136.

(37) Han, Y.; Xu, Z.; Gao, C. Ultrathin Graphene Nanofiltration Membrane for Water Purification. *Adv. Funct. Mater.* **2013**, *23* (29), 3693–3700.

(38) Wei, N.; Peng, X.; Xu, Z. Understanding Water Permeation in Graphene Oxide Membranes. *ACS Appl. Mater. Interfaces* **2014**, *6* (8), 5877–5883.

(39) Nam, Y. T.; Choi, J.; Kang, K. M.; Kim, D. W.; Jung, H. T. Enhanced Stability of Laminated Graphene Oxide Membranes for Nanofiltration via Interstitial Amide Bonding. *ACS Appl.*

Mater. Interfaces **2016**, *8* (40), 27376–27382.

(40) Miyamoto, A.; Kuwaki, Y.; Sano, T.; Hatakeyama, K.; Quitain, A.; Sasaki, M.; Kida, T. Solid Electrolyte Gas Sensor Based on a Proton-Conducting Graphene Oxide Membrane. *ACS Omega* **2017**, *2* (6), 2994–3001.

(41) Choi, S.; Goryll, M.; Sin, L. Y. M.; Wong, P. K.; Chae, J. Microfluidic-Based Biosensors toward Point-of-Care Detection of Nucleic Acids and Proteins. *Microfluid. Nanofluid.* **2011**, *10* (2), 231–247.

(42) Pulizzi, F.Building a Better Nanopore. *Nat. Nanotechnol.* **2016**, *11* (2), 105–105.

(43) Nair, R. R.; Wu, H. A.; Jayaram, P. N.; Grigorieva, I. V.; Geim, A. K. Unimpeded Permeation of Water Through Helium-Leak-Tight Graphene-Based Membranes. *Science* **2012**, *335* (6067), 442–444.

(44) Chen, C.; Yang, Q. H.; Yang, Y.; Lv, W.; Wen, Y.; Hou, P. X.; Wang, M.; Cheng, H. M. Self-Assembled Free-Standing Graphite Oxide Membrane. *Adv. Mater.* **2009**, *21* (29), 3007–3011.

(45) Lam, Y.; Lail, N. I. A.; Alam, M. S.; Zauscher, S. Using Microcantilever Deflection to Detect HIV-1 Envelope Glycoprotein gp120. *Nanomedicine (N. Y., NY, U. S.)* **2006**, *2* (4), 222–229.

(46) Lee, J. H.; Oh, B. K.; Choi, J. W. Electrochemical Sensor Based on Direct Electron Transfer of HIV-1 Virus at Au Nanoparticle Modified ITO Electrode. *Biosens. Bioelectron.* **2013**, *49*, 531–535.

(47) Chen, W.; Feng, Y.; Prabakaran, P.; Ying, T.; Wang, Y.; Sun, J.; Macedo, C. D. S.; Zhu, Z.; He, Y.; Polonis, V. R.; Dimitrov, D. S. Exceptionally Potent and Broadly Cross-Reactive, Bispecific Multivalent HIV-1 Inhibitors Based on Single Human CD4 and Antibody Domains. *J. Virol.* **2014**, *88* (2), 1125–1139.

(48) Chen, W.; Gong, R.; Ying, T.; Prabakaran, P.; Zhu, Z.; Feng, Y.; Dimitrov, D. Discovery of Novel Candidate Therapeutics and Diagnostics Based on Engineered Human Antibody Domains. *Curr. Drug Discovery. Technol.* **2014**, *11* (1), 28–40.

(49) Chen, W.; Xiao, X.; Wang, Y.; Zhu, Z.; Dimitrov, D. S. Bifunctional Fusion Proteins of the Human Engineered Antibody Domain m36 with Human Soluble CD4 Are Potent Inhibitors of Diverse HIV-1 Isolates. *Antiviral Res.* **2010**, *88* (1), 107–115.

(50) Rauti, R.; Lozano, N.; León, V.; Scaini, D.; Musto, M.; Rago, I.; Ulloa Severino, F. P.; Fabbro, A.; Casalis, L.; Vázquez, E.; Kostarelos, K.; Prato, M.; Ballerini, L. Graphene Oxide Nanosheets Reshape Synaptic Function in Cultured Brain Networks. *ACS Nano* **2016**, *10* (4), 4459–4471.

(51) Marcano, D. C.; Kosynkin, D. V.; Berlin, J. M.; Sinitskii, A.; Sun, Z.; Slesarev, A.; Alemany, L. B.; Lu, W.; Tour, J. M. Improved Synthesis of Graphene Oxide. *ACS Nano* **2010**, *4* (8), 4806–4814.

(52) Hu, W.; Peng, C.; Luo, W.; Lv, M.; Li, X.; Li, D.; Huang, Q.; Fan, C. Graphene-Based Antibacterial Paper. *ACS Nano* **2010**, *4* (7), 4317–4323.

(53) Peng, S.; Fan, X.; Li, S.; Zhang, J. Green Synthesis and Characterization of Graphite Oxide by Orthogonal Experiment. *J. Chil. Chem. Soc.* **2013**, *58* (4), 2213–2217.

(54) Chen, J.; Yao, B.; Li, C.; Shi, G. An Improved Hummers Method for Eco-Friendly Synthesis of Graphene Oxide. *Carbon* **2013**, *64* (1), 225–229.

(55) Oger, N.; Lin, Y. F.; Labrugère, C.; Grognec, E. L.; Rataboul, F.; Felpin, F. X. Practical and Scalable Synthesis of Sulfonated Graphene. *Carbon* **2016**, *96*, 342–350.

(56) Daly, M.; Cao, C.; Sun, H.; Sun, Y.; Filleter, T.; Singh, C. V. Interfacial Shear Strength of Multilayer Graphene Oxide Films. *ACS Nano* **2016**, *10* (2), 1939–1947.

(57) Ray, S. C. Application and Uses of Graphene. In *Applications of Graphene and Graphene-Oxide Based Nanomaterials*; Elsevier, 2015; pp 39–55.

(58) Dikin, D. A.; Stankovich, S.; Zimney, E. J.; Piner, R. D.; Dommett, G. H. B.; Evmenenko, G.; Nguyen, S. T.; Ruoff, R. S. Preparation and Characterization of Graphene Oxide Paper.

Nature **2007**, *448* (7152), 457–460.

(59) Cui, P.; Lee, J.; Hwang, E.; Lee, H. One-Pot Reduction of Graphene Oxide at Subzero Temperatures. *Chem. Commun. (Cambridge, U. K.)* **2011**, *47* (45), 12370.

(60) Pires, L. B.; Martínez, C. C. M.; Sánchez, M. M.; Montón, H.; Merkoçi, A. Water Activated Graphene Oxide Transfer Using Wax Printed Membranes for Fast Patterning of a Touch Sensitive Device. *ACS Nano* **2016**, *10* (1), 853–860.

(61) Hu, M.; Mi, B. Enabling Graphene Oxide Nanosheets as Water Separation Membranes. *Environ. Sci. Technol.* **2013**, *47* (8), 3715–3723.

(62) Singh, K. P.; Dhek, N. S.; Nehra, A.; Ahlawat, S.; Puri, A. Applying Graphene Oxide Nano-Film over a Polycarbonate Nanoporous Membrane to Monitor E. Coli by Infrared Spectroscopy. *Spectrochim. Acta, Part A* **2017**, *170*, 14–18.

(63) Ghorbel, E.; Hadriche, I.; Casalino, G.; Masmoudi, N. Characterization of Thermo-Mechanical and Fracture Behaviors of Thermoplastic Polymers. *Materials* **2014**, *7* (1), 375–398.

(64) Kim, K. Chemical and Electrical Characterization of Virgin and Protein-Fouled Polycarbonate Track-Etched Membranes by FTIR and Streaming-Potential Measurements. *J. Membr. Sci.* **1997**, *134* (2), 199–208.

(65) Huang, K.; Liu, G.; Shen, J.; Chu, Z.; Zhou, H.; Gu, X.; Jin, W.; Xu, N. High-Efficiency Water-Transport Channels Using the Synergistic Effect of a Hydrophilic Polymer and Graphene Oxide Laminates. *Adv. Funct. Mater.* **2015**, *25* (36), 5809–5815.

(66) Cressiot, B.; Oukhaled, A.; Patriarche, G.; Gallego, M. P.; Betton, J. M.; Auvray, L.; Muthukumar, M.; Bacri, L.; Pelta, J. Protein Transport through a Narrow Solid-State Nanopore at High Voltage: Experiments and Theory. *ACS Nano* **2012**, *6* (7), 6236–6243.

(67) Kowalczyk, S. W.; Tuijtel, M. W.; Donkers, S. P.; Dekker, C. Unraveling Single-Stranded DNA in a Solid-State Nanopore. *Nano Lett.* **2010**, *10* (4), 1414–1420.

(68) Tansel, B.; Sager, J.; Rector, T.; Garland, J.; Strayer, R. F.; Levine, L.; Roberts, M.; Hummerick, M.; Bauer, J. Significance of Hydrated Radius and Hydration Shells on Ionic Permeability during Nanofiltration in Dead End and Cross Flow Modes. *Sep. Purif. Technol.* **2006**, *51* (1), 40–47.

(69) Wang, Y.; Bai, X.; Wen, W.; Zhang, X.; Wang, S. Ultrasensitive Electrochemical Biosensor for HIV Gene Detection Based on Graphene Stabilized Gold Nanoclusters with Exonuclease Amplification. *ACS Appl. Mater. Interfaces* **2015**, *7* (33), 18872–18879.

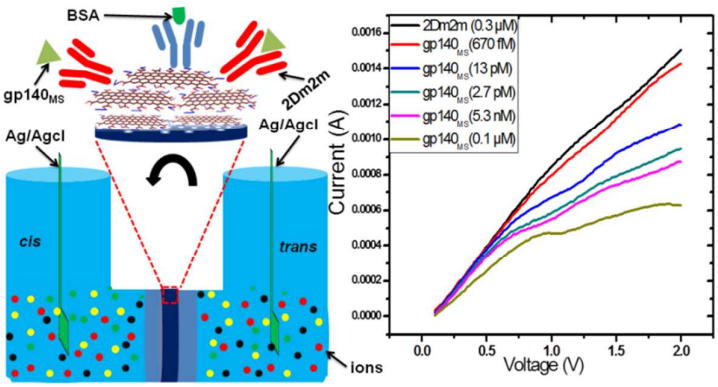
BSA
gp140MS
2Dm2m
Ag/AgCl
Ag/AgCl
cis
trans
ions
2Dm2m (0.3 μM)
gp140MS (670 fM)
gp140MS (13 pM)
gp140MS (2.7 pM)
gp140MS (5.3 nM)
gp140MS (0.1 μM)
Current (A)
Voltage (V)
0.0016
0.0014
0.0012
0.0010
0.0008
0.0006
0.0004
0.0002
0.0000
0.0
0.5
1.0
1.5
2.0

TOC Graphic